Neurobiology of Disease

Tip60's Novel RNA-Binding Function Modulates Alternative Splicing of Pre-mRNA Targets Implicated in Alzheimer's Disease

Akanksha Bhatnagar,[1] Keegan Krick,[2*] Bhanu Chandra Karisetty,[1*] Ellen M. Armour,[1] Elizabeth A. Heller,[2] and Felice Elefant[1]

[1]Department of Biology, Drexel University, Philadelphia, Pennsylvania 19104 and [2]Department of Systems Pharmacology and Translational Therapeutics, University of Pennsylvania, Philadelphia, Pennsylvania 19104

The severity of Alzheimer's disease (AD) progression involves a complex interplay of genetics, age, and environmental factors orchestrated by histone acetyltransferase (HAT)-mediated neuroepigenetic mechanisms. While disruption of Tip60 HAT action in neural gene control is implicated in AD, alternative mechanisms underlying Tip60 function remain unexplored. Here, we report a novel RNA binding function for Tip60 in addition to its HAT function. We show that Tip60 preferentially interacts with pre-mRNAs emanating from its chromatin neural gene targets in the *Drosophila* brain and this RNA binding function is conserved in human hippocampus and disrupted in *Drosophila* brains that model AD pathology and in AD patient hippocampus of either sex. Since RNA splicing occurs co-transcriptionally and alternative splicing (AS) defects are implicated in AD, we investigated whether Tip60-RNA targeting modulates splicing decisions and whether this function is altered in AD. Replicate multivariate analysis of transcript splicing (rMATS) analysis of RNA-Seq datasets from wild-type and AD fly brains revealed a multitude of mammalian-like AS defects. Strikingly, over half of these altered RNAs are identified as bona-fide Tip60-RNA targets that are enriched for in the AD-gene curated database, with some of these AS alterations prevented against by increasing Tip60 in the fly brain. Further, human orthologs of several Tip60-modulated splicing genes in *Drosophila* are well characterized aberrantly spliced genes in human AD brains, implicating disruption of Tip60's splicing function in AD pathogenesis. Our results support a novel RNA interaction and splicing regulatory function for Tip60 that may underly AS impairments that hallmark AD etiology.

Key words: alternative splicing; Alzheimer's disease; histone acetylation; neuroepigenetics; RNA; Tip60

Significance Statement

Alzheimer's disease (AD) has recently emerged as a hotbed for RNA alternative splicing (AS) defects that alter protein function in the brain yet causes remain unclear. Although recent findings suggest convergence of epigenetics with co-transcriptional AS, whether epigenetic dysregulation in AD pathology underlies AS defects remains unknown. Here, we identify a novel RNA interaction and splicing regulatory function for Tip60 histone acetyltransferase (HAT) that is disrupted in *Drosophila* brains modeling AD pathology and in human AD hippocampus. Importantly, mammalian orthologs of several Tip60-modulated splicing genes in *Drosophila* are well characterized aberrantly spliced genes in human AD brain. We propose that Tip60-mediated AS modulation is a conserved critical posttranscriptional step that may underlie AS defects now characterized as hallmarks of AD.

Received Dec. 21, 2022; revised Feb. 8, 2023; accepted Feb. 13, 2023.

Author contributions: A.B. and F.E. designed research; A.B. performed research; A.B. and E.M.A. contributed unpublished reagents/analytic tools; A.B., K.K., B.C.K., E.A.H., and F.E. analyzed data; A.B. and F.E. edited the paper; A.B. and F.E. wrote the paper.

The research was supported by the National Institutes of Neurological Disorders and Stroke of the National Institutes of Health under Award Number R01NS095799 (to F.E.). We thank Dr. Ann Ehrenhofer-Murray for generously contributing the *Drosophila*-Tip60 antibody. We also thank Dr. Harini Sreenivisappa for overseeing microscopic imaging at Drexel University's Cell Imaging Center.

*K.K. and B.C.K. contributed equally to this work and are co-second authors.

The authors declare no competing financial interests.

Correspondence should be addressed to Felice Elefant at fe22@drexel.edu.

https://doi.org/10.1523/JNEUROSCI.2331-22.2023

Introduction

Alzheimer's Disease (AD) is a chronic late-onset neurodegenerative disorder characterized by an accumulation of amyloid plaques and neurofibrillary tangles, memory impairment and cognitive decline (DeTure and Dickson, 2019; Knopman et al., 2021). The severity of AD progression is dependent in large part, by epigenetic histone acetylation mediated neural gene control mechanisms (Sanchez-Mut and Gräff, 2015; Killin et al., 2016; Nativio et al., 2018). Reduced histone acetylation resulting from decreased histone acetyltransferase (HAT) and/or increased histone deacetylase (HDAC) activity causes chromatin packaging

alterations in neurons with concomitant transcriptional dysregulation that is a key initial step in AD etiology (Francis et al., 2009; Gräff et al., 2012; Peixoto and Abel, 2013; Lu et al., 2014). In this regard, we previously identified a neuroprotective role by the Tip60 HAT in AD (Zhu et al., 2007; Pirooznia et al., 2012; Johnson et al., 2013; Pirooznia and Elefant, 2013; Xu et al., 2014, 2016; Panikker et al., 2018; Karnay et al., 2019; H. Zhang et al., 2020; Beaver et al., 2021; Bhatnagar et al., 2023). Increasing Tip60 HAT levels in the brains of *Drosophila* that model AD-associated neurodegeneration protects against AD associated neuroepigenetic deficits that include reduced Tip60 and enhanced HDAC2 chromatin enrichment and concomitant transcriptional dysregulation and ameliorates multiple AD-associated phenotypes including Aβ plaque accumulation, neural apoptosis, synaptic plasticity, learning/memory, and longevity. Intriguingly, recent insights reveal that histone modifying enzymes, such as HDACs, not only determine which genes are expressed but also how the transcribed RNA is ultimately spliced (Luco et al., 2011; Rahhal and Seto, 2019; Agirre et al., 2021). Thus, while the role of Tip60 HAT activity in chromatin-mediated gene expression is well established, it remains to be studied whether Tip60 has the ability to modulate alternative splicing (AS) decisions that may in part contribute toward its neuroprotective abilities.

In addition to the catalytic HAT domain, Tip60 also contains an N-terminus chromodomain that acts as a code reader that recognizes distinct methylated-lysine histone tails (Sun et al., 2009; C.H. Kim et al., 2015). Elegant studies have shown that chromodomains within certain proteins have the ability to directly interact with RNA that likely aids in chromosomal recruitment and targeting (Akhtar et al., 2000; Bernstein and Allis, 2005; Morales et al., 2005; Bernstein et al., 2006; Shimojo et al., 2008; Ishida et al., 2012; Akoury et al., 2019). Interestingly, a closely related HAT belonging to the same MYST superfamily as Tip60, MOF, is dependent on its chromodomain-RNA binding for integration into chromosomal complexes and dosage compensation (Akhtar et al., 2000). Tip60 chromodomain has also been shown to be critical for its recruitment to chromatin-rich regions in human cell lines as chromodomain mutations cause Tip60 mislocalization (Sun et al., 2009; C.H. Kim et al., 2015). Additionally, chromatin-interacting heterochromatin protein 1 (HP1) has been recently shown to modulate alternative splicing decisions via its direct RNA binding function (Rachez et al., 2021). However, it remains to be elucidated whether Tip60 has RNA binding capabilities and if so, whether Tip60-RNA binding aid in chromatin recruitment and/or splicing modulation.

Here, we uncover a novel RNA binding function for Tip60 HAT that underlies RNA alternative splicing (AS) regulation in the brain. Genome-wide RNA immunoprecipitation (RIP) and sequencing of Tip60-bound RNA from *Drosophila* brain reveal Tip60 specifically targets RNAs enriched for critical neuronal processes implicated in AD. Strikingly, Tip60 targets pre-mRNA emanating from its chromatin gene targets and this function is conserved in human hippocampal tissues and disrupted in both *Drosophila* AD-brains that model AD pathology and in AD patient hippocampal samples. Over half of these Tip60 interacting RNAs from AD fly brains exhibit a multitude of mammalian-like AS defects enriched for in the AD-gene curated database. Notably, some splicing alterations are partially protected against by increasing Tip60 in the AD fly brain, suggesting that Tip60 modulates AS decisions for AD-associated RNA targets. Our results support an RNA splicing regulatory function for Tip60 that modulates AS decisions for its unspliced pre-mRNA targets and that disruption of this Tip60 function in the AD brain may underly AS impairments that hallmark AD etiology.

Table 1. Primer sequences used for human RIP-qPCR

No.	Tip60 RNA target	Human ortholog	Forward primer	Reverse primer
1	Adar	ADARB1	AAGCTGCCTTGGGATCAGAG	GACACGTTGTCCAGATTGCG
2	CG32809	KIAA1217	GCAGAACTCCAGGCATTCCA	TCCATTTGGGGGCCATTTTC
3	dlg1	DLG1	GGTATGTGCGCCTTGGATCT	AAGGTGCAATGCTCTCTGGG
4	Dscam1	DSCAML1	TTTCAACAAGATTGGCCGCAG	AATCTGGTAGCCCCGGATGA
5	fs(1)h	BRD2	ATACGGGTGTGCCTTTGGG	TCCTCAAACTCCATTCCGGC
6	HDAC4	HDAC4	TGGAGTGGGGAGAAGCATCA	TCCAACGAGCTCCAAACTCC
7	heph	PTBP1	CTGCGCATCGACTTTTCCAA	AGGCTGAGATTATACCAGGTGC
8	kuz	ADAM10	ACCACAGACTTCTCCGGAATC	GGTCTGTGAAGACATAGGCCA
9	Nckx30C	SLC24A2	CTTCCAAACAGCACCAGCAC	GACTTGCTTGCGGGTTTCAG
10	Rab3-GEF	MADD	AAAGCATCAAACCCGGACCT	ACAAAGACGCCTCGAACTGT
11	Rbfox1	RBFOX1	GAGGGCCGTAAAATCGAGGT	AAGCCTGGCACTGCATAGAA
12	trol	HSPG2	ATACGATGGCTTGTCTCTGCC	GTCGTCTCCTGAGATGCTGTC
13	GAPDH	GAPDH	TCGGAGTCAACGGATTTGGT	TTCCCGTTCTCAGCCTTGAC

Materials and Methods

Fly stocks and crosses

All fly lines were raised under standard conditions at 25°C with 12/12 h light/dark cycle on yeasted *Drosophila* media (Applied Scientific Jazz Mix *Drosophila* Food, Thermo Fischer Scientific). The w^{1118}, pan-neuronal driver *elav^{C155}-Gal4,* transgenic UAS lines carrying human APP695 isoform (*UAS-APP^{695}*), and Tip60-RNAi-mediated knock-down *(UAS-Tip60 RNAi)* were all obtained from Bloomington Drosophila Stock Center. Generation and characterization of the double-transgenic *UAS-APP^{695}; Tip60^{WT}* fly lines are described previously (Pirooznia et al., 2012). The *elav^{C155}-Gal4* driver line was crossed with either w^{1118} (wild-type control), *UAS-APP^{695}* (APP model), *UAS-APP^{695}; Tip60^{WT}* (APP; Tip60 model), or *UAS-Tip60 RNAi* (Tip60 RNAi model). For all experiments, transgene expression levels for APP and/or Tip60 in each UAS fly lines were revalidated using a quality control qPCR strategy with RNA extracted from the same pooled larval brains used for RNA immunoprecipitation and sequencing (RIP-Seq) or RIP-qPCR experiments. Although all transgenic fly lines have been well characterized with appropriate controls, we do not rule out the unpredictable physiological changes associated with addition of P[w+] transgene for generation of fly lines.

Homology modeling and molecular visualization

3D protein structure of *Drosophila* Tip60 chromodomain was generated using SWISS-MODEL automated protein structure homology modeling server (Waterhouse et al., 2018). X-ray crystallized structure of *Homo sapiens* Tip60 chromodomain (PDB: 4QQG, chain A) with 79% coverage was used as a modeling template. After energy-minimization with YASARA Energy Minimization Server (Krieger et al., 2009) and stereochemical quality checks with ProCheck server (Laskowski et al., 1993), the resultant *Drosophila* Tip60 chromodomain model was exported as a PDB file. All visualization and molecular alignments were performed using PyMOL molecular viewing software (DeLano, 2002).

In silico *RNA target predictions*

Tip60's RNA interaction probabilities were calculated using the RNA-protein interactions prediction (RPISeq) server (Muppirala et al., 2011). RNA sequences of key genes involved in synaptic plasticity were obtained from the NCBI database. Input protein sequences containing either only the chromodomain region or the full protein *Drosophila* Tip60 protein (Q960X4) were submitted. Each interaction was scored between 0 and 1 using support vector machine (SVM) classifier.

Multiple sequence alignment and secondary structure prediction

Protein sequences of Esa1 in *Saccharomyces cerevisiae* (Q08649) and Tip60 from *Drosophila melanogaster* (Q960X4), *H. sapiens* (Q92993), *Pongo abelii*

Table 2. Primer sequences used for splice-specific qPCR in Tip60 RNAi-mediated knock-down

No.	Tip60 RNA target	Splicing event	Transcript	Transcript RefSeq ID	Forward primer	Reverse primer
1	heph	Skipped exon	Exon 6 present	NM_001260470.1	GCAGTGGGTGGTGGTACAAT	TGTTCGTCGATCCTTACCTTTT
			Exon 6 spliced out	NM_001104522.3	CAACGTGTGCAAATCAAACTCGAA	GTTCGTCGATCCTTACCTTAACTC
2	dlg1	Alternative 5′ splice site	Exon 1 long isoform	NM_001272518.1	TGGGTGTGTTGTTTTCGTCG	TTATCCAACTTTTTGCATTGTGTTC
			Exon 1 short isoform	NM_001258694.2	TCGATTCTACTAGTTGGTGCAA	TGGCGTTCGAGGGTTAAAGT
3	Rab3-GEF	Alternative 3′ splice site	Exon 4 long isoform	NM_001103513.3	TCCGGGTAATGGTGGACCT	GTTAAGAGGCCGTAACTGCTA
			Exon 4 short isoform	NM_001347809.1	TCGGCATTTAGCAGCGACT	GAGTGGTGTGAGTGTAGGCG
4	Dscam1	Mutually exclusive exons	First exon 6 included	NM_001043023.1	ACCGACGCCTATGATGGAAA	ACTTATCTTGGGGCTGACTGTG
			Second exon 6 included	NM_001259237.1	AGGCAGCGAATACGATGGAA	GAGTGTCCACTTTGGGAGCC
5	Adar	Retained intron	Intron 3_4 spliced out	NM_001258547.2	ACGCGAGTTACTACATGCCT	TGGTGCACTCACCGGTTTTA
			Intron 3_4 retained	NM_001258548.2	TGAGATGCCAAAATACTCTGATCC	GTGTACCGGACCAGTCTGTG
6	Rpl32			NM_170461.3	TGGTTTCCGGCAAGCTTCAA	TGTTGTCGATACCCTTGGGC

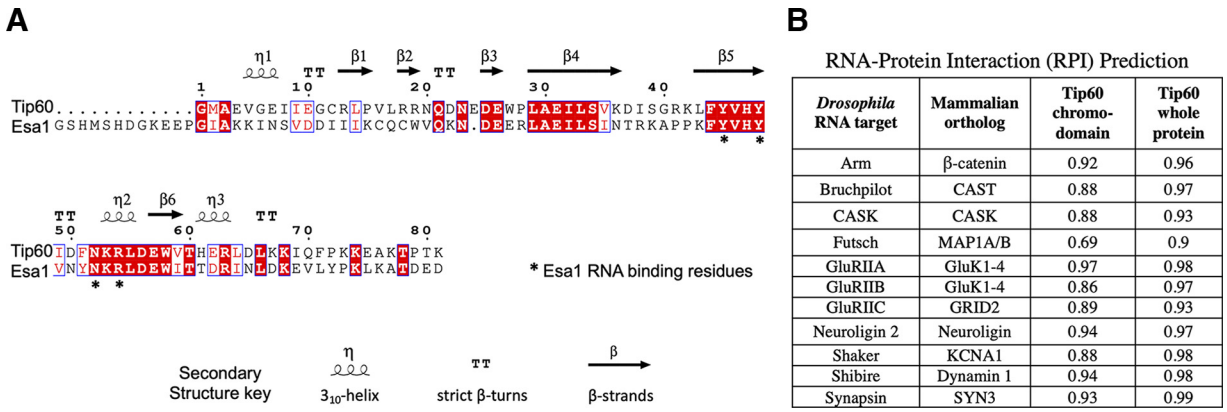

Figure 1. Tip60 secondary structure conservation with Esa1 HAT and putative RNA targets. ***A***, Tip60 chromodomain is predicted to fold in a similar secondary structure as Esa1 chromodomain with conserved RNA-binding helical turn ($\eta 2$) and four proven RNA-binding residues from Esa1 (denoted with *). *Drosophila melanogaster* Tip60 (Q960X4) and *Saccharomyces cerevisiae* Esa1 (Q08649) sequence similarities and secondary structure information were analyzed using ESPript. ***B***, Several key mRNA involved in synaptic plasticity are putative Tip60 targets. RNA-protein interactions prediction (RPISeq) server was used to score *Drosophila* Tip60 (Q960X4) protein interactions with mRNA candidates. A probability of >0.5 suggests a strong possibility of the mRNA candidates being a target of the Tip60 chromodomain or the full protein, respectively.

(*Sumatran orangutan*; Q5RBG4), *Mus musculus* (Q8CHK4), and *Rattus norvegicus* (Q99MK2) were obtained from UniProt Knowledgebase (UniProt Consortium, 2020). Protein sequences were aligned using Clustal Omega multiple sequence alignment tool (Sievers et al., 2011) with default parameters. Alignment results were visualized using Jalview bioinformatics software (Waterhouse et al., 2009). Secondary structure predictions were performed using protein sequence alignment of yeast Esa1 and *Drosophila* Tip60 on the "Easy Sequencing in PostScript" (ESPript) program (Robert and Gouet, 2014).

Polytene chromosome squashes, staining, and imaging

Polytene chromosomes (PC) were prepared from wild-type third instar larvae and were fixed and stained according to conventional squash technique using acid fixation as previously described (Johansen et al., 2009). For RNase treatment, salivary glands were incubated in PBS with 0.4% PBT for 5 min and RNase (500 μg/ml, Thermo Scientific EN0531) for 15 min before proceeding with fixation. Primary antibodies used were guinea-pig anti-dTip60 (1:5000; from Schirling et al., 2010), mouse anti-RNA polymerase-II (1:400, Sigma: 05-623), and rabbit anti-acetyl-histone H3 antibody (1:400, Sigma 06-599). Secondary antibodies used were Alexa Flour 488, 568, and 633 (Invitrogen) at 1:200. DNA on chromosomes was counterstained using DAPI dye. Confocal microscopy was performed using laser scanning Fluoview Olympus microscope (FV-1000, Olympus Lifesciences) at 60× magnification using z-stacks. Sequential scanning mode was used to detect fluorophores in two different phases to avoid cross talk. Images were processed using ImageJ software.

rMATS splicing analysis

For splicing analysis, clean reads from Input samples were aligned to the *Drosophila melanogaster* genome (Ensembl version BDGP6) using STAR (Dobin et al., 2013). Splice isoform switching events were detected using replicate Multivariate Analysis of Transcript Splicing (rMATS; S. Shen et al., 2014). Alternative splicing was quantified using the percent spliced in (PSI) metric that reports inclusion or splicing of an event such that PSI = Inclusion/(Inclusion + Exclusion). For genotypic comparisons, differences in relative isoform abundance were calculated as ΔPSI values: $\Delta PSI(APP \text{ vs wild-type}) = PSI_{APP} - PSI_{wild\text{-}type}$; and $\Delta PSI(APP;Tip60 \text{ vs } APP) = PSI_{APP;Tip60} - PSI_{APP}$. Positive ΔPSI values indicate higher inclusion in APP over wild-type and APP;Tip60 over APP, respectively. Significant splicing events were identified using the cutoffs: false discovery rate (FDR) < 0.1 and $|\Delta PSI| \geq 0.1$. Conserved human orthologs were predicted using best match from DRSC integrative ortholog prediction tool (DIOPT; Hu et al., 2011).

RNA immunoprecipitation and sequencing (RIP-Seq)

Magna RIP RNA-binding protein immunoprecipitation kit (Millipore) was used for native, more direct RNA immunoprecipitation without protein cross-linking. A total of 200 *Drosophila* third instar larval brains were dissected in ice-cold PBS and teased apart with a Dounce homogenizer. The tissue was resuspended in RIP lysis buffer after centrifugation at 1500 rpm for 5 min. In each tissue lysate sample, 10% fraction was kept aside for total RNA purification (INPUT RNA) and the remaining 90% were used for RNA immunoprecipitation (IP RNA). Magnetic beads were prepared according to the protocol using rabbit-Tip60 antibody (Abcam ab23886, 7.5 μg), and normal rabbit IgG (7.5 μg) was used as a negative control. The pretreated beads and tissue lysate were mixed and incubated with rotation overnight at 4°C. After washing with RIP wash buffer for five times, protein was digested using proteinase K treatment. RNA was phenol– chloroform precipitated from IP and INPUT samples in parallel. RNA purity and integrity were assessed using Nanodrop spectrophotometer (Thermo Fisher

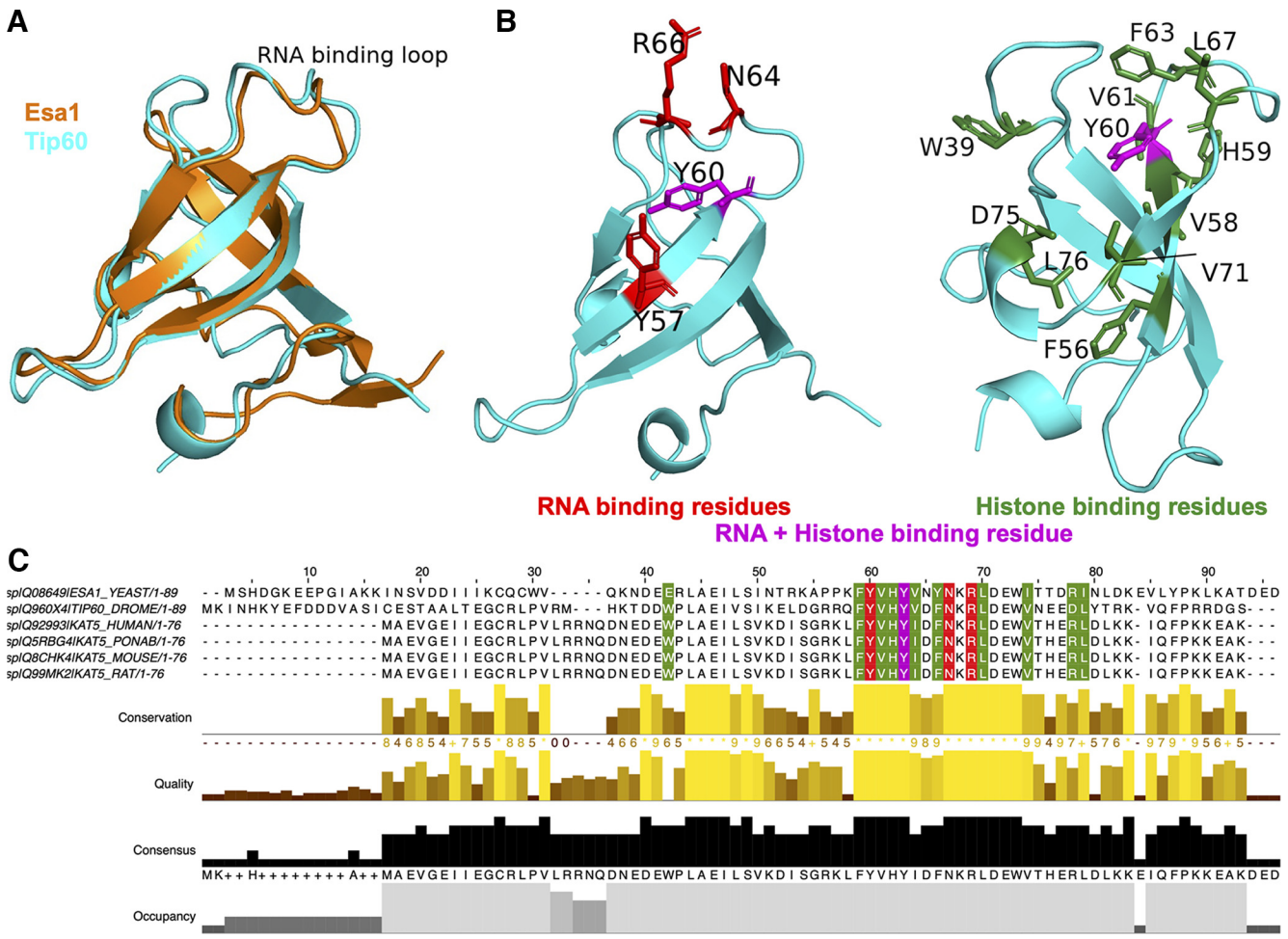

Figure 2. Tip60's structural homology with known RNA-binding Esa1 HAT uncovers distinct conserved RNA-binding and histone-binding sites. ***A***, Structural homology between *Drosophila* Tip60 chromodomain (cyan, SWISS-MODEL) and known RNA-binding yeast Esa1 chromodomain (orange, PDB: 2Ro0). ***B***, Amino acid residues in the *Drosophila* Tip60 chromodomain predicted for RNA binding (red), histone binding (green), or both functions (magenta). ***C***, Evolutionary conservation of chromodomain RNA-binding and histone-binding residues across mammalian species. Multiple sequence alignment with Clustal Omega was used to align *Drosophila* Tip60 chromodomain (UniProt: Q960X4) with Esa1 yeast (Q08649) and Tip60 from *Homo sapiens* (Q92993), *Pongo abelii* (Sumatran orangutan; Q5RBG4), *Mus musculus* (Q8CHK4), and *Rattus norvegicus* (Q99MK2).

Scientific) and RNA 6000 Nano assay on 2100 Bioanalyzer (Agilent Technologies). Whole transcriptome sequencing was performed on IP and INPUT RNA samples using DNBSEQ sequencing technology platform (BGI Genomics, China) with 100-bp paired-end reads. Low-quality raw reads were filtered out using in-house BGI genomics pipeline on SOAPnuke (BGI-flexlab; Chen et al., 2018). Clean RNA reads were aligned to the *Drosophila melanogaster* genome (Ensembl version BDGP6) using HISAT2 (D. Kim et al., 2019). Reads were mapped using Bowtie2 (Langmead and Salzberg, 2012) and gene expression was quantified using RNA-Seq by expectation-maximization (RSEM; B. Li and Dewey, 2011). Principal component analysis (PCA) and heatmap clustering (Euclidean distance) were performed to cluster the samples and identify the batch effects and sample heterogeneity. All plots were constructed using R/Bioconductor. Gene ontology biological processes and human disease relevance was assessed using FlyEnrichr, a gene list enrichment analysis tool for *D. melanogaster* (Chen et al., 2013). Read distribution was assessed using Resect RNA-seq Quality Control package (Wang et al., 2012) on individual BAM files and *Drosophila* dm6 RefSeq genome bed file (O'Leary et al., 2016), and the output was visualized using MultiQC modular tool (Ewels et al., 2016).

RNA immunoprecipitation and RT-qPCR (RIP-qPCR) on human hippocampal tissues

For all human studies, human hippocampal samples were obtained from the National Disease Research Interchange (NDRI), with informed consent by all donors. The control brains included three males with an age range of 70–85 years. The AD brains were from one male and two females with an age range of 73–87 years. For RNA Immunoprecipitation, frozen hippocampal tissues were disrupted in liquid nitrogen using Cryo-Cup Grinder (BioSpec Products). Lysate were processed with either rabbit-Tip60 antibody (Abcam ab23886, 7.5 μg) or normal rabbit IgG (7.5 μg). Protein was digested using proteinase K treatment and RNA was phenol–chloroform precipitated. For RT-qPCR analysis, cDNA was prepared using the SuperScript II reverse transcriptase kit (Invitrogen) according to the manufacturer's instructions with 1 µg of total RNA. RT-qPCRs were performed in a 10 µl reaction volume containing cDNA, 1 μM Power SYBR Green PCR Master Mix (Applied Biosystems), and 10 μM forward and reverse primers. Primers are listed in Table 1. RT-qPCR was performed using an ABI 7500 Real-Time PCR system (Applied Biosystems) following the manufacturer's instructions. Fold enrichment for all the respective genes was calculated relative to the nonspecific rabbit IgG antibody control.

Splice-specific qPCR

Total RNA was isolated from 40 staged third instar larval brains using the Quick-RNA Miniprep kit (Zymo Research). cDNA was prepared using the SuperScript II reverse transcriptase kit (Invitrogen) according to the manufacturer's instructions with 1 µg of total RNA. Isoform specific exon-exon junction primers were designed using NCBI Primer-BLAST. The primer pair specificity was analyzed using the reference sequence database of *D. melanogaster* (taxid: 7227). RT-qPCRs were

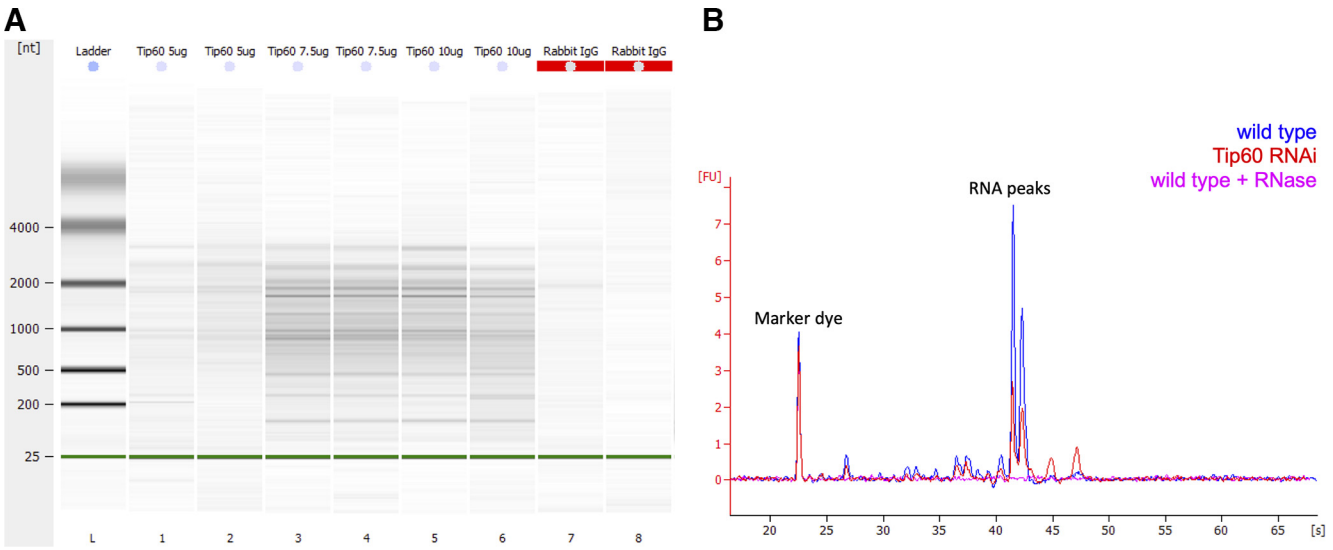

Figure 3. Tip60-RNA immunoprecipitation (RIP) assay controls. ***A***, Bioanalyzer gel shows immunoprecipitated RNA at specific nucleotide sizes with increasing Tip60 antibody concentrations of 5 μg (lanes 1, 2), 7.5 μg (lanes 3, 4), and 10 μg (lanes 5, 6). RNA is not immunoprecipitated with Rabbit IgG control (lanes 7, 8). RNA is separated based on nucleotide sizes from larger molecules at top to smaller molecules at bottom. ***B***, Tip60-RNAi-mediated knock-down reduces amount of RNA immunoprecipitated (red) when compared with wild-type (blue). Sample peak is lost after RNase treatment of wild-type sample (magenta), confirming presence of RNA in the immunoprecipitate samples. RNA migration time (seconds, *x*-axis) of constant marker dye and samples are plotted against fluorescence intensity (*y*-axis). RNA concentration is determined based on the time corrected area underneath each sample peak and the upper marker in each sample. [nt]: nucleotide sizes; [FU]: fluorescence intensity.

performed in a 10-µl reaction volume containing cDNA, 1 μM Power SYBR Green PCR Master Mix (Applied Biosystems), and 10 μM forward and reverse primers. Primers are listed in Table 2. RT-qPCR was performed using an ABI 7500 Real-Time PCR system (Applied Biosystems) following the manufacturer's instructions. Fold change in mRNA expression was determined by the δ-δCt method relative to wild type using Rpl32 as housekeeping gene.

Experimental design and statistical analysis

All statistical analysis were performed using GraphPad Prism version 9.4.0 software package. Statistical analysis of RNA-Seq data differences between two groups were considered statistically significant with $q < 0.05$ [false discovery rate (FDR) < 0.05, controlled by Benjamini–Hochberg]. For identification of Tip60-RNA targets significantly enriched in IP over Input, a threshold cutoff of adjusted p-value < 0.05 was used. Volcano plots comparing Tip60's RNA targets significantly enriched in wild type, APP, and APP;Tip60 were generated using a threshold cutoff of adjusted p-value < 0.05 and $\log_2$ Fold Change of ≤ -0.583 and ≥ 0.583). Alternative splicing events significantly altered between genotypes were identified using FDR < 0.1. Volcano plots depicting difference in relative isoform abundance between genotypes were generated using a threshold cutoff of FDR < 0.1 and $|\Delta PSI| \geq 0.1$, where PSI = percent spliced in. For splice-specific RT-qPCR, statistical significance between the two groups was calculated using unpaired Student's t test with $p < 0.05$. For Tip60 IP fold enrichment in healthy versus AD human tissues, two-way ANOVA with Sidak's multiple comparison test was used with $p < 0.05$.

Results

Structural homology and evolutionary conservation of *Drosophila* Tip60 RNA binding residues across mammalian species supports their critical functional significance

Chromodomains are protein–RNA interaction modules (Akhtar et al., 2000), yet it remains to be determined whether the Tip60 chromodomain structure is primed for an RNA-binding function. Structural studies on Esa1 HAT, the common ortholog of Tip60 and MOF HATs in yeast, have mapped its RNA-binding activity to a specific helical turn structural motif (η2) in its chromodomain (Shimojo et al., 2008). Using protein secondary structure predictions, we found structural conservation between Tip60 and Esa1 chromodomains, especially at the RNA-binding helical turn motif (η2; Fig. 1*A*). Similarly, protein structure superimposition shows Tip60 chromodomain folds into an almost identical 3D structure as the Esa1 chromodomain with minimal structural divergence of 1.02 root mean square deviation (Fig. 2*A*). Importantly, Tip60 chromodomain contains the predicted tudor-knot conformation and the RNA-binding helical turn motif essential for RNA-binding in Esa1 (Shimojo et al., 2008), supporting functional similarity for putative Tip60-RNA binding. Since Tip60 plays a crucial role in synaptic plasticity (Sarthi and Elefant, 2011; Beaver et al., 2020), we next assessed whether key mRNA involved in synaptic plasticity are predicted to interact with the Tip60 chromodomain and full protein. Using the *in silico* RNA-protein interaction prediction server (Muppirala et al., 2011), we identified several mRNA candidates strongly predicted to interact with the Tip60 chromodomain (Fig. 1*B*). These results support an RNA-binding function for Tip60's chromodomain that is predicted to target mRNA enriched for synaptic plasticity.

Prior work using Esa1 mutational screens identified four precise RNA-binding residues in the chromodomain that completely abolished Esa1's RNA-binding ability when mutated (Shimojo et al., 2008). Notably, these four RNA-binding residues were found to be conserved in Tip60's chromodomain and are exposed at the surface near the RNA-binding turn (Fig. 2*B*). The polar nature of all four amino acids, Tyr 57, Tyr 60, Asn64, and Arg66, suggests these residues interact with RNA via hydrogen bonding, which is a typical characteristic of protein-RNA interactions (Teplova et al., 2011; Corley et al., 2020). Additionally, the positively charged Arg66 is able to complement the negatively charged RNA for ionic bonding, another common observation with protein-RNA binding (Chen and Varani, 2005). In contrast, the proven and predicted Tip60's histone-binding residues- Trp39, Phe56, Val58, His59, Tyr60, Val61, Phe63, Leu67, Val71, Asp75, Leu76 (Sun et al., 2009;

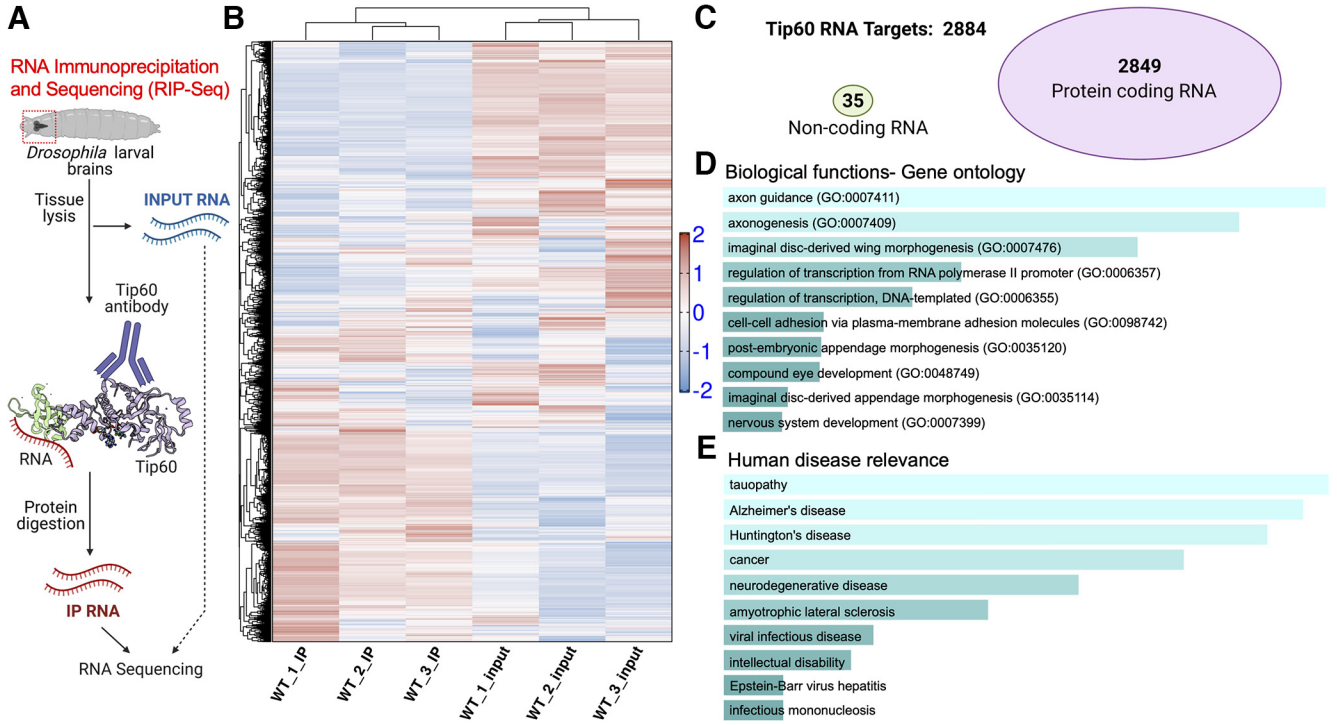

Figure 4. RNA Immunoprecipitation and Sequencing (RIP-Seq) reveals a highly specific, selective, and reproducible RNA-binding function for Tip60 in the *Drosophila* brain. ***A***, RIP-Seq schematic: Tip60-bound RNA molecules are immunoprecipitated and extracted (IP RNA) along with the total RNA (INPUT RNA) from *Drosophila* larval brains for RNA Sequencing. ***B***, Hierarchically clustered heatmap depicting RNA homogeneity within replicates and variability between IP and INPUT groups from three wild-type (WT) biological replicates. ***C***, Classification of Tip60 RNA targets as protein coding or noncoding RNA. ***D***, Gene ontology biological processes and (***E***) human diseases enriched for the top 2000 Tip60 RNA targets. Refer to Extended Data Table 4-1 for Tip60 RNA targets significantly enriched in IP and Extended Data Table 4-2 for Gene Ontology analysis and human disease relevance.

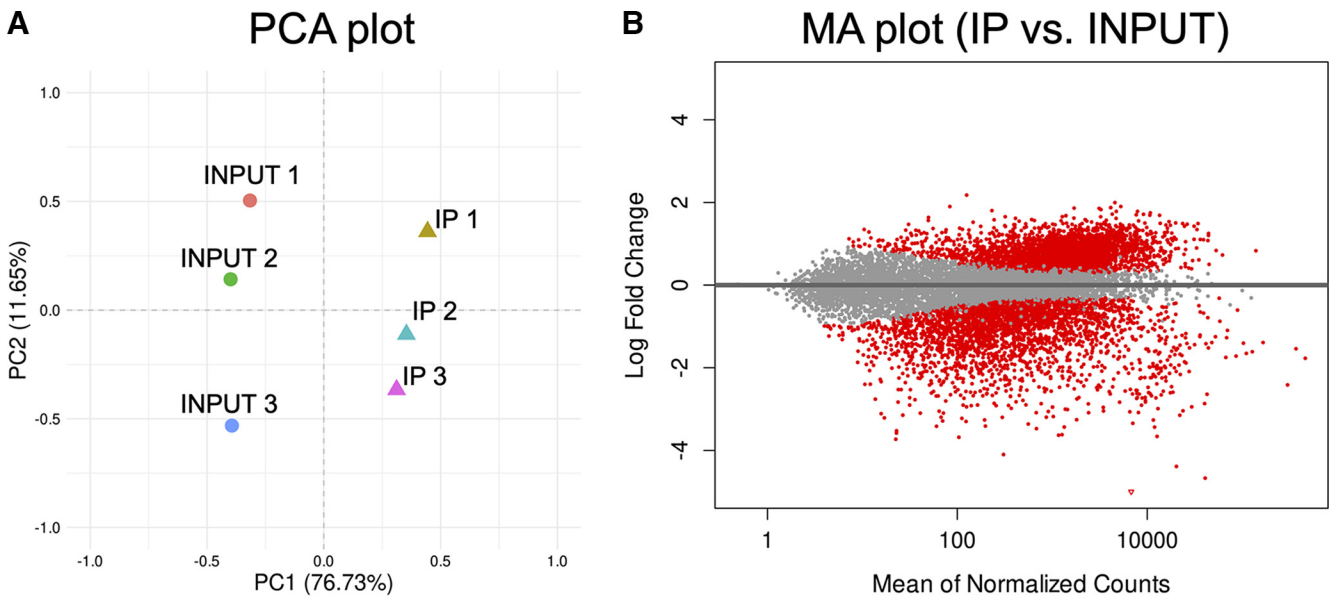

Figure 5. Tip60-RNA target identification in the wild-type (WT) samples. ***A***, Principal component analysis (PCA) plot showing samples variation between RNA enriched in the IP samples (triangles) and respective Input samples (circles) from three wild-type (WT) *Drosophila* biological replicates. ***B***, MA scatter plot shows log fold change of IP RNA over Input RNA (*y*-axis) and average expression between the groups (*x*-axis). Red scatters are present below the threshold cutoff of adjusted *p*-value < 0.05. WT: wild type; IP: immunoprecipitate RNA; INPUT: Input RNA.

Letunic and Bork, 2018; Y. Zhang et al., 2018) are mostly nonpolar amino acid residues positioned inside the chromodomain core. Specifically, Tyr60, and Phe63 amino acids together form an aromatic cage in the Tip60 chromodomain that recognizes methylated lysine residues for histone acetylation (Y. Zhang et al., 2018). The close proximity of RNA-binding residues with this aromatic cage and the indispensable role of Tyr60 in both, RNA-binding (Shimojo et al., 2008) and histone-binding functions (Sun et al., 2009) suggests that these two functions do not occur simultaneously. Lastly, all RNA-binding residues and

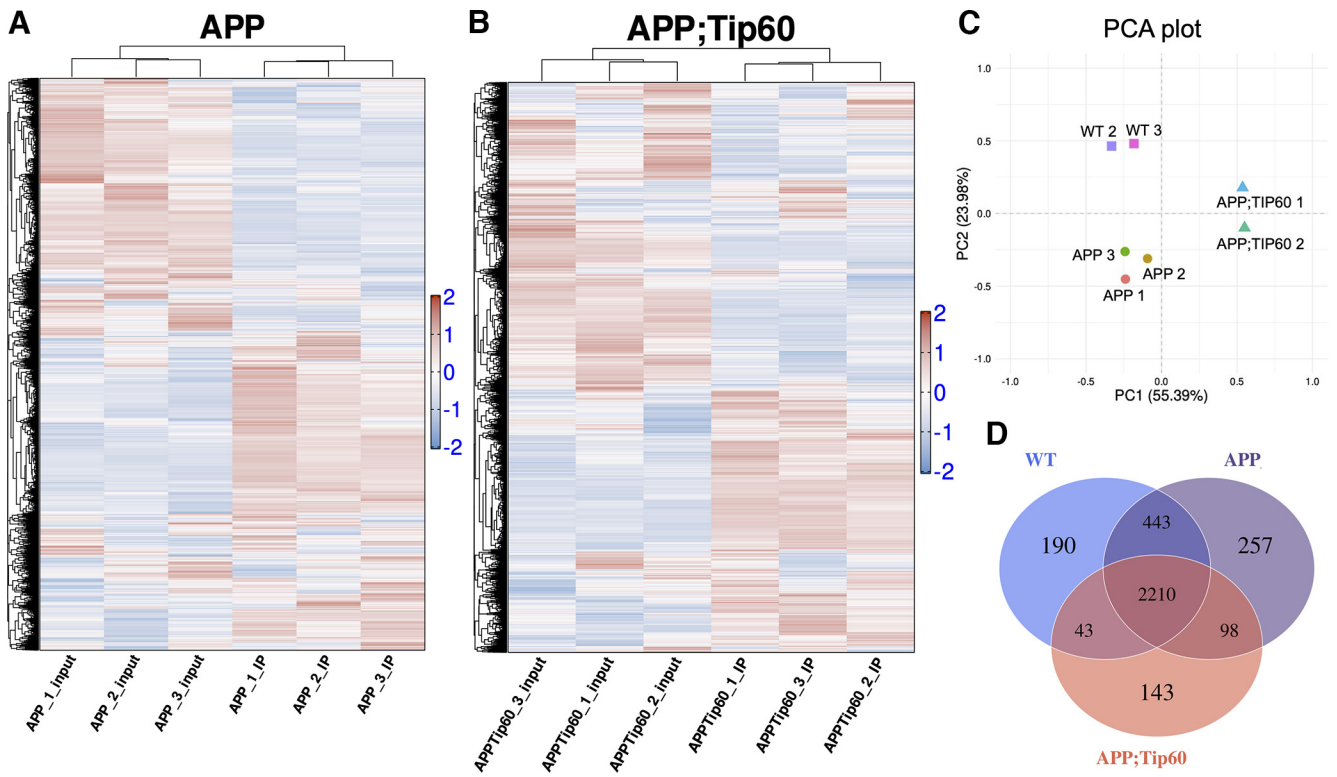

Figure 6. Tip60's RNA targets comparison between *Drosophila* wild-type, APP, and APP;Tip60 conditions. Heatmap depicting RNA enriched in IP and INPUT biological replicates from (***A***) APP and (***B***) APP;Tip60 *Drosophila* larval brains. ***C***, Principal component analysis (PCA) plot showing variation between Tip60's RNA targets that are specifically enriched in the immunoprecipitate RNA (IP RNA) between the wild-type (square), APP (circles), and APP;Tip60 (triangles). ***D***, Venn diagram shows distribution of Tip60's RNA targets that are unique or shared between wild type (blue), APP (purple), and APP;Tip60 (red). WT: wild type; IP: immunoprecipitate RNA; Input: Input RNA.

most histone binding residues were found to be evolutionary conserved across mammalian species, indicating their functional importance (Fig. 2*C*). Together, these results strongly support a novel, conserved RNA-binding function for Tip60 chromodomain that is likely mutually exclusive from its well-studied histone-binding function.

Tip60 interacts with protein encoding RNAs enriched for neuronal processes implicated in cognition and neurodegenerative disorders *in vivo*

Since our structural and molecular findings support an RNA-binding function for the Tip60 chromodomain, we asked whether Tip60 directly interacts with RNA molecules *in vivo*. For genome- centric identification of Tip60-RNA interactions, we used a noncrosslinking, native RNA immunoprecipitation (RIP) technique to extract Tip60-bound RNA from wild-type *Drosophila* larval brains. We confirmed the presence of RNA molecules in the Tip60-immunoprecipitate that revealed RNAs at specific nucleotide size (~100–2000 base pairs) in different biological replicates (Fig. 3*A*). Notably, RNA was not detected with nonspecific rabbit IgG and less RNA was immunoprecipitated with RNAi-mediated Tip60 knock-down, indicating Tip60's RNA binding is specific *in vivo* (Fig. 3*B*). Further, nucleic acid bands were completely lost after RNase treatment, confirming presence of RNA in the immunoprecipitate samples. Our results uncover a specific and reproducible RNA-binding function for Tip60 in *Drosophila* brain, *in vivo*.

To identify Tip60's RNA targets *in vivo*, we performed whole transcriptome sequencing (RIP-Seq) on both the Tip60-immunoprecipiated RNA (IP RNA) and total RNA present in tissue before immunoprecipitation (Input RNA) for enrichment comparison (Fig. 4*A*). Heatmap of RNA enrichment across samples shows two important observations (Fig. 4*B*). First, similar RNAs are immunoprecipitated in all three IP RNA samples, indicative of highly specific Tip60-RNA interaction. Second, several RNAs enriched in the Input RNA were not immunoprecipitated in the IP RNA, suggesting Tip60 does not equally favor binding to all RNA molecules. Next, we performed a principal component analysis (PCA) to observe variation between the samples (Fig. 5*A*). As expected, the IP RNA and Input RNA samples clustered in two separate groups, suggesting limited sample-to-sample variation. In contrast, there was major variation between the IP and Input RNA clusters, validating that Tip60's RNA binding function is highly selective and reproducible in different biological samples. To further confirm Tip60's RNA-binding selectivity, we used the MA scatter plot that shows log fold change of IP over Input RNA (Fig. 5*B*). Using a threshold cutoff of adjusted p-value < 0.05, we identified RNAs significantly different between IP and Input (red scatters). We then selected for RNAs significantly enriched in IP over input, which we refer to as "Tip60 RNA targets." Our RIP-Sequencing identified a total of 2884 Tip60-RNA targets, of which 35 are noncoding RNAs and 2849 are protein encoding RNAs (Fig. 4*C*; Extended Data Table 4-1). To study biological pathways and disease relevance of the top 2000 Tip60 RNA targets, we used FlyEnrichr, a gene list enrichment analysis tool for *D. melanogaster* (Chen et al., 2013). Our analysis revealed that Tip60 RNA targets were enriched for critical dynamic neuronal processes that included axon guidance and axonogenesis, transcription and development (Fig. 4*D*). Notably, the majority of these processes are linked to several

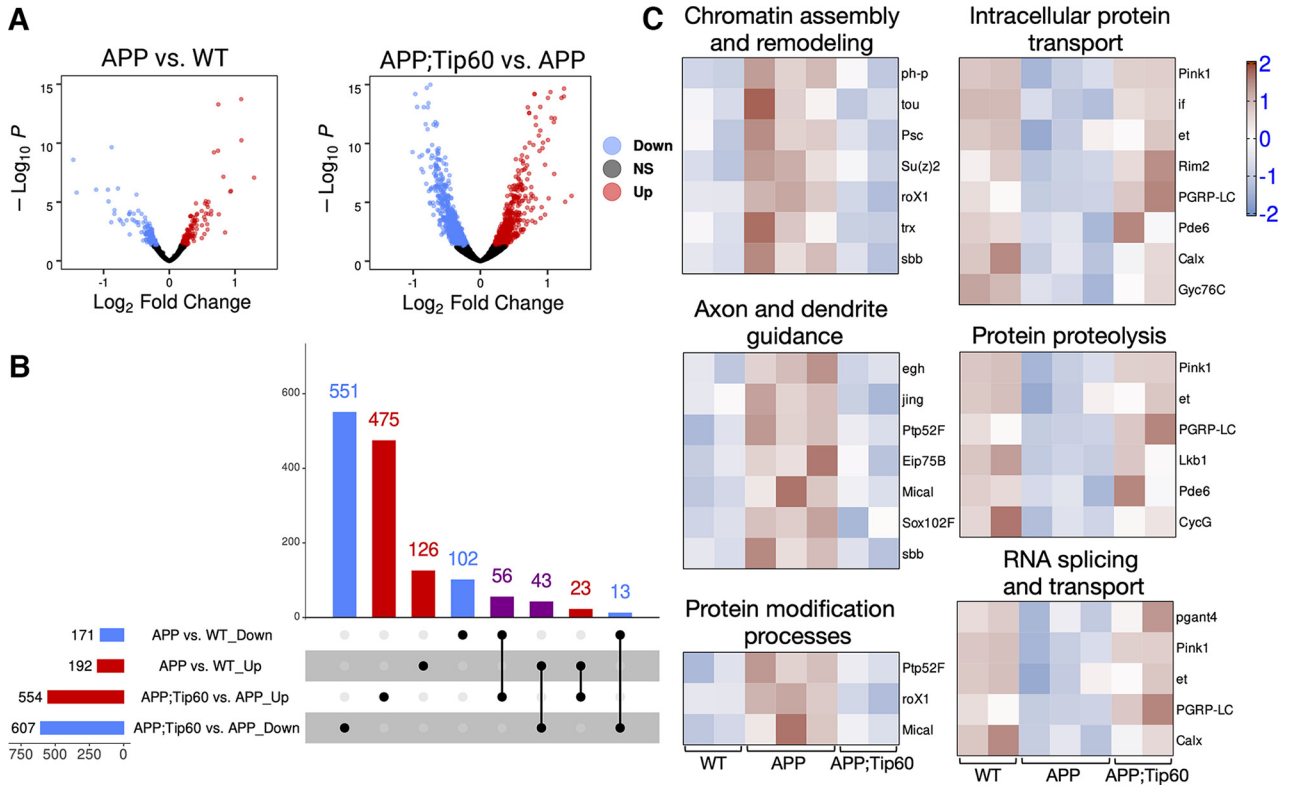

Figure 7. Tip60 RNA targets are altered in *Drosophila* APP neurodegenerative model and partially rescued by Tip60 overexpression. ***A***, Volcano plots depicting Tip60's RNA targets specifically enriched in immunoprecipitate RNA (IP RNA) between APP versus wild-type (left) and APP;Tip60 versus APP (right) *Drosophila* larval brains. Tip60-RNA targets with significantly enriched binding (red), reduced binding (blue) or nonsignificant binding alterations (black) between genotypes are depicted (cutoff: adjusted *p*-value < 0.05; $\log_2$ fold change of ≤ -0.583 and ≥ 0.583). ***B***, UpSet plot representing the distribution and intersection of Tip60's RNA target alterations between APP versus wild type and APP;Tip60 versus APP. Rows represent the total number of Tip60-RNA targets in each comparison that are either unique (black dots) or overlapping (connecting line) with other comparisons. Purple columns represent Tip60 rescued RNA targets. ***C***, Biological pathways enriched for Tip60-rescued RNA targets that are either excluded in wild-type, targeted in APP, and excluded again in APP;Tip60 (left) or targeted in wild type, excluded in APP, and targeted again in APP;Tip60 (right). Some genes appear in more than one GO category. WT: wild type; NS: not significant. See Extended Data Table 7-1 for Tip60's RNA targets comparison between *Drosophila* wild-type, APP, and APP;Tip60 conditions.

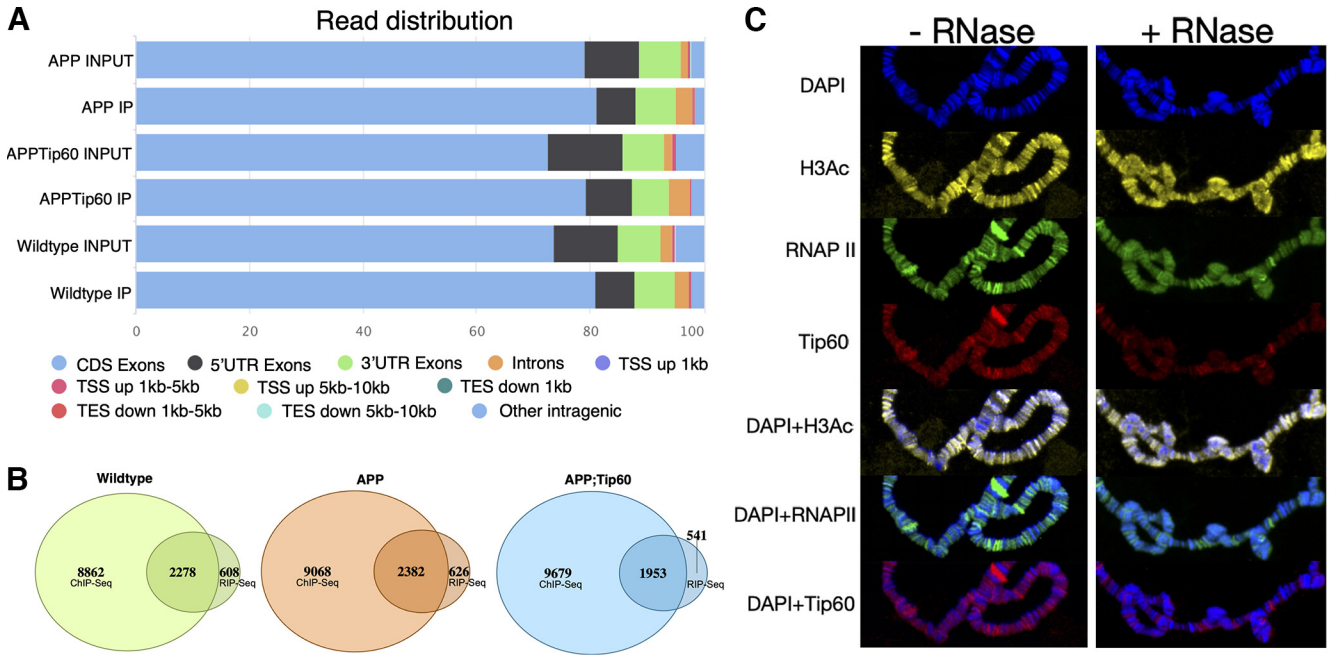

Figure 8. Tip60 targets identical gene loci at chromatin and RNA levels. ***A***, Reads from Tip60-immunoprecipitated RNA (IP) and total RNA (Input) samples in wild type, APP, and APP;Tip60 were mapped to corresponding genomic features in the following priority order: CDS exons (blue) > UTR exons (black/green) > Introns (orange) > Intergenic regions. CDS: coding DNA sequence; TSS: transcription start site; TES: transcription end site. ***B***, Overlap between Tip60's RNA targets and its gene targets identified via chromatin immunoprecipitation and sequencing (ChIP-Seq) in wild-type, APP, and APP;Tip60 *Drosophila* larval brains. ***C***, *Drosophila* salivary polytene chromosomes stained for DAPI (blue), histone H3 pan-acetyl (yellow), RNA polymerase-II (green), and Tip60 (red) antibodies wither in the presence or absence of RNase. Refer to Extended Data Table 8-1 for overlap between Tip60's RNA targets and gene targets at the chromatin level.

human diseases with tauopathy and Alzheimer's Disease displaying highest prevalence (Fig. 4*E*; Extended Data Table 4-2). Together, our results identify a highly specific RNA-binding function for Tip60 in the brain *in vivo* that favors interaction with protein encoding RNAs that mediate critical neuronal processes linked to neurodegenerative diseases.

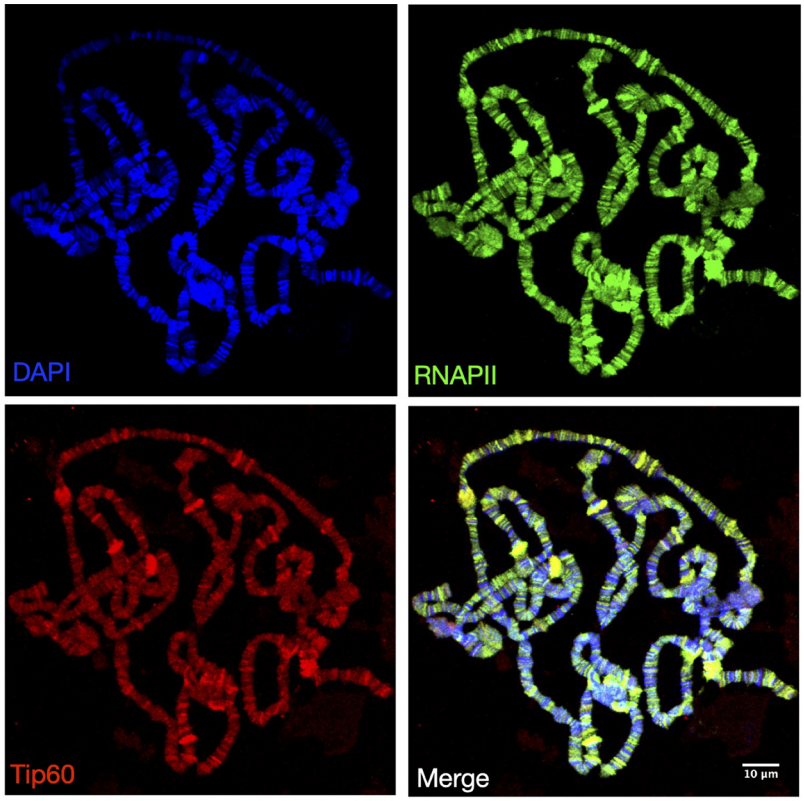

Figure 9. Tip60 localizes to the actively transcribed gene regions on polytene chromosomes. Polytene chromosomes from wild-type *Drosophila* salivary glands are squashed and co-stained with DAPI (blue), RNA polymerase-II (green), and Tip60 (red). Tip60 co-localizes with RNA polymerase II in the interbands region (merged yellow) representing sites of active gene transcription between densely packed heterochromatin. RNAPII: RNA-polymerase II.

Increased Tip60 partially rescues Tip60-RNA targeting alterations in the APP AD associated neurodegenerative brain

We previously showed that early-preclinical mild cognitive impairments (MCI) and late-stage AD pathologies in humans are tightly conserved both epigenetically and pathologically in the extensively characterized AD associated human amyloid precursor protein (APP) *Drosophila* model (APP AD; Zhu et al., 2007; Pirooznia et al., 2012; Johnson et al., 2013; Pirooznia and Elefant, 2013; Xu et al., 2014, 2016; Panikker et al., 2018; Karnay et al., 2019; Beaver et al., 2020, 2021; H. Zhang et al., 2020; Bhatnagar et al., 2023). This high degree of disease conservation allows for general principles learned from the AD APP fly to be applied to mammalian systems. Our prior studies revealed reduced Tip60 HAT levels with concomitant altered patterns of chromatin histone acetylation and neuronal gene expression in the brains of our APP AD *Drosophila* model that contribute to cognitive deficits and are prevented by increased Tip60 levels. Thus, we asked whether Tip60's RNA-binding function is also perturbed in APP AD flies and that this defect can be ameliorated by genetically increasing Tip60 levels. To address this question, we assessed Tip60-RNA interactions under pan-neuronally expressed human APP^{695} isoform alone (APP AD model) or in combination with Tip60 wild-type protein (APP;Tip60 model) using RIP-Seq on *Drosophila* larval brains. Transcriptomic sequencing of Tip60-IP RNA and Input RNA revealed that similar to wild-type, Tip60-RNA binding is specific and selective for only certain RNA molecules from the entire Input RNA pool in APP and APP;Tip60 genotypes (Fig. 6*A*,*B*). Further, using a threshold cutoff of adjusted p-value < 0.05, we identified Tip60 RNA targets enriched in IP that clustered separately between genotypes, suggesting variations in Tip60-RNA binding in different genotypes (Fig. 6*C*; Extended Data Table 4-1). Although the majority of RNA targets are shared by all three genotypes, we found certain RNAs that are uniquely targeted only in wild-type, APP, or APP;Tip60, supporting Tip60 RNA target divergence in different genotypes (Fig. 6*D*). Together, these results demonstrate that although specificity and selectivity of Tip60's RNA binding functions remains unaltered, Tip60 targets partially different sets of RNA in wild-type, APP, and APP;Tip60 *Drosophila* models.

To better understand how Tip60's RNA-binding function is altered in different genotypes, we compared the distribution and intersection of Tip60's RNA targets between APP versus wild-type and APP versus APP;Tip60 (Extended Data Table 7-1). Using volcano plot analysis, we first identified Tip60's RNA targets that are significantly enriched in IP in APP (red scatters), wild-type (blue scatters), or both (black scatters; Fig. 7*A*, left) and APP;Tip60 (red scatters), APP (blue scatters), or both (black scatters; Fig. 7*A*, right). We found similar number of Tip60-RNA targets that are either significantly enriched or depleted in binding in APP versus wild-type (192 and 171, respectively) and APP;Tip60 versus APP (554 and 607, respectively). Next, we used an UpSet plot to visualize intersections between these four differential Tip60-RNA target comparisons that are represented as individual rows (Fig. 7*B*). Out of the 171 RNA that interacted with Tip60 in wild-type but not in APP brains (row 1), increased Tip60 in the APP;Tip60 genotype restored Tip60-RNA interactions with 56 (32.8%) of these RNAs (row 1 and row 3 overlap, purple bar). Similarly, out of the 192 RNA that Tip60 mistargeted in APP but not in wild-type (row 2), increased Tip60 in the APP;Tip60 genotype resulted in reduced inappropriate interactions in 43 (22.4%) of these RNAs (row 2 and row 4 overlap, purple bar). Together, increased Tip60 in the APP;Tip60 genotype restored 27.6% (99/363) Tip60-RNA target interactions that were altered in the APP brain that we refer to as 'Tip60 rescued RNA targets'. To identify the biological processes these Tip60 rescued RNA targets are involved in, we performed functional annotation clustering on this set of RNAs using FlyEnrichr gene ontology analysis (Fig. 7*C*). Top enriched cellular processes included chromatin assembly and remodeling, axon and dendrite guidance, protein modification, intracellular transport, and proteolysis, and intriguingly, RNA transport and splicing. Together, our results point to a functional role for Tip60-RNA binding in the brain that is disrupted under APP neurodegenerative conditions and is partially protected against by increased Tip60.

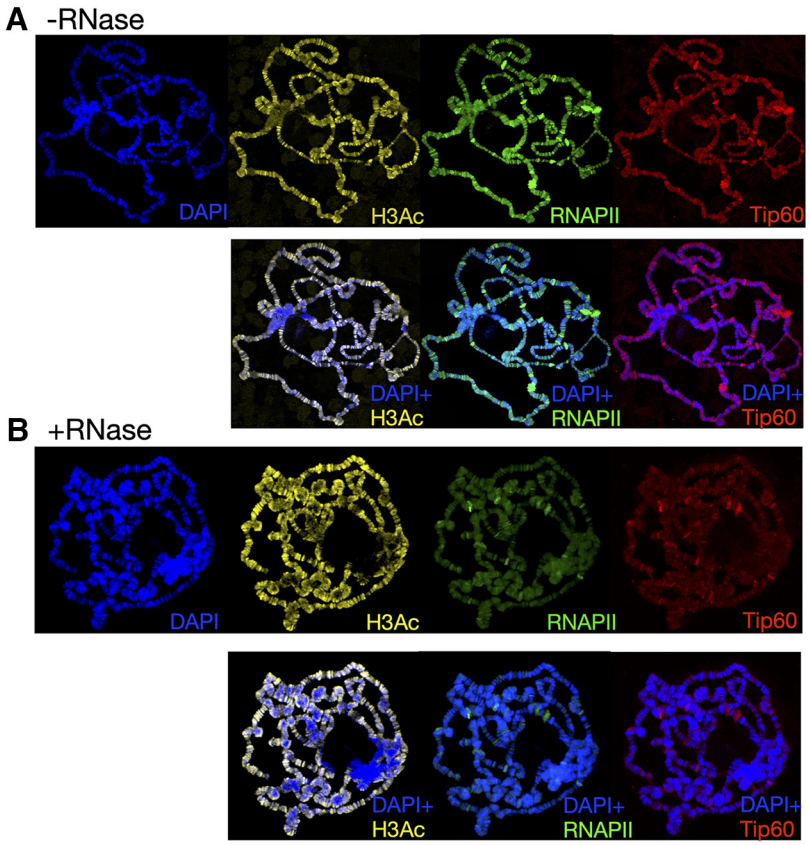

Figure 10. Tip60's chromatin recruitment is sensitive to RNase treatment. Polytene chromosomes from wild-type *Drosophila* salivary glands were squashed and co-stained with DAPI (blue), histone H3 pan-acetyl (yellow), RNA polymerase-II (green), and Tip60 (red) antibodies. ***A***, In absence of RNase treatment, polytene chromosomes are saturated with histone H3 pan-acetyl, RNA polymerase-II, and Tip60 staining. ***B***, After RNase treatment, RNA polymerase-II, and Tip60 staining are partially lost while histone H3 pan-acetylation staining remains unaffected on polytene chromosomes. RNAPII: RNA-polymerase II; H3Ac: histone H3 pan-acetylation.

Tip60 interacts with pre-mRNAs that emanate from Tip60's chromatin gene targets

We previously reported that Tip60 displays a nuclear cytoplasmic distribution pattern in both the *Drosophila* and mammalian brain. Thus, we asked whether Tip60 primarily interacts with unspliced pre-mRNA in the nucleus or mature spliced mRNA in the cytoplasm. We performed RSEQC read distribution analysis (Wang et al., 2012) on our Tip60-IP RNA and Input RNA samples from RIP-Seq to calculate the distribution pattern of mapped reads over different genome features, such as like coding DNA sequence (CDS) exon, 5′ untranslated region (UTR) exon, 3′ UTR exon, intron, and intergenic regions (Fig. 8*A*). As expected from the Input samples containing both pre-mRNA and mature mRNA, the majority of the reads mapped to CDS exonic regions and UTR regions, while the remaining mapped to introns and intergenic regions. Strikingly, we observed similar read distribution in Tip60-IP RNA samples, including mapping to intronic regions, suggesting the presence of pre-mRNA in the RNA population that Tip60 specifically interacts with. Further, read mapping at intronic regions revealed higher enrichment of RNAs from Tip60-RIP samples when compared with their respective Inputs for all genotypes, indicating that Tip60 preferentially targets unspliced pre-mRNAs that reside in the nucleus. Finally, since RNA splicing is predominantly co-transcriptional and occurs in close proximity with the chromatin loci it originates with, we asked whether there is any overlap between Tip60 target RNAs and chromatin gene loci. To address this question, we compared our Tip60 RNA targets from RIP-Seq with Tip60 chromatin gene targets we previously published using ChIP-Seq (Beaver et al., 2021). Importantly, RIP-Seq and CHIP-Seq were performed using identical staged larval brains for wild-type, APP, and APP;Tip60 genotypes. Remarkably, we observed a significant overlap (78–79%) between Tip60's RNA and gene targets for wild-type ($p < 2.263e-06$), APP ($p < 7.115e-17$), and APP;Tip60 ($p < 6.523e-28$, hypergeometric test; Fig. 8*B*; Extended Data Table 8-1). These results suggest that Tip60 regulates identical genes at both the chromatin and RNA level, potentially by interacting with nascent RNA as it is transcribed.

The significant overlap between Tip60's gene targets at the chromatin and RNA level prompted us to ask whether Tip60's interaction with RNA is required for its chromatin interaction. To address this question, we assessed whether RNase treatment misclocalizes Tip60 in polytene chromosomes (PCs) within fly salivary glands. PCs are a well-established model to study functional chromosomes because of large size and prominent banding pattern (Johansen et al., 2009; Vatolina et al., 2011). As expected, we found that *Drosophila* Tip60 localizes to the less-compact interbands in PCs, representing regions of highly active gene transcription (Fig. 9; Schirling et al., 2010) and accordingly, co-localizes with RNA Pol II. Treatment of PCs with RNase reduced Tip60 staining, supporting a putative role for Tip60-RNA interaction occurring in close proximity to chromatin (Figs. 8*C*, 10). Together, our results demonstrate that Tip60 primarily targets identical gene loci at both the chromatin and RNA level and that Tip60's RNA binding function is at least in part, required for Tip60's chromatin interaction.

Tip60 mediates alternative splicing selection of neural pre-mRNA targets associated with Alzheimer's disease

Our published ChIP studies showing Tip60 chromatin enrichment at intergenic and intronic regions within genes (Beaver et al., 2021) in conjunction with our RNA read map analysis revealing enrichment of RNAs within intronic regions of these same genes in Tip60- RIP samples support an interaction between Tip60 and unspliced pre-mRNAs. In neurons, AS of pre-mRNA is a central mechanism used to increase the genetic plasticity and proteomic diversity required for dynamic neuronal processes, making these tissues particularly suspectable to splicing defects (Q. Li et al., 2007; Su et al., 2018). Given that AS is primarily co-transcriptional and that AS defects hallmark AD, we hypothesized that Tip60-RNA interaction mediates AS of pre-mRNA targets emanating from Tip60's chromatin gene loci and that this process is disrupted in the APP AD larval brain. To assess Tip60's involvement in potential AS defects in the APP brain, we applied replicate multivariate analysis of transcript splicing (rMATS) analysis on RNA-Sequencing data from *Drosophila* wild-type, APP, and APP;Tip60 Input samples (Extended Data

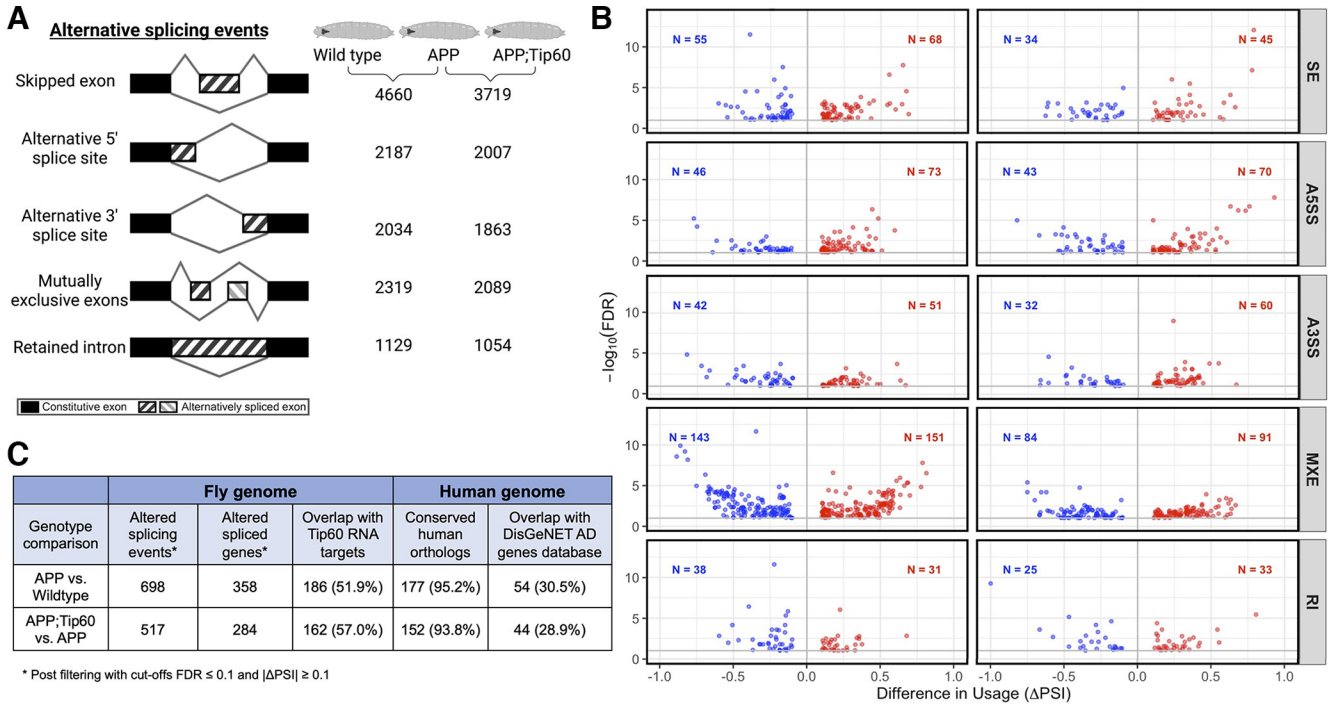

C

Genotype comparison	Fly genome			Human genome	
	Altered splicing events*	Altered spliced genes*	Overlap with Tip60 RNA targets	Conserved human orthologs	Overlap with DisGeNET AD genes database
APP vs. Wildtype	698	358	186 (51.9%)	177 (95.2%)	54 (30.5%)
APP;Tip60 vs. APP	517	284	162 (57.0%)	152 (93.8%)	44 (28.9%)

* Post filtering with cut-offs FDR ≤ 0.1 and |ΔPSI| ≥ 0.1

Figure 11. Tip60-RNA targets differentially spliced in *Drosophila* APP and APP;Tip60 models are implicated in Alzheimer's disease (AD). ***A***, Summary of total differential alternative splicing events detected between APP versus wild type and APP;Tip60 versus APP using rMATS. Alternative splicing events are classified as Skipped Exons (SE), Alternative 5′ Splice Site (A5SS), Alternative 3′ Splice Site (A3SS), Mutually Exclusive Exons (MXE), and Retained Intron (RI). ***B***, Volcano plot depicting splicing events significantly altered between APP versus wild-type (left) and APP;Tip60 versus APP (right) *Drosophila* larval brains. The relative abundance of each isoform was quantified as percentage spliced in (PSI) for every genotype; ΔPSI (*x*-axis) quantified the difference in relative isoform abundance between different genotypes. All events are significant [false discovery rate (FDR) $<$ 0.1 and $|\Delta PSI| \geq 0.1$]. ***C***, Significantly altered splicing events were mapped to fly genome and filtered for direct Tip60 RNA targets identified via RIP-Seq in wild type. Conserved human orthologs were predicted using DIOPT and compared with DisGeNET database for AD relevance. See Extended Data Tables 11-1 and Tables 11-2 for complete splicing results from rMATS analysis between APP versus wild-type and APP;Tip60 versus APP.

Table 11-1, Table 11-2). The relative abundance of each isoform was quantified as percentage spliced in (PSI); ΔPSI quantified the difference in relative isoform abundance between genotypes. Our analysis uncovered a multitude of differential mammalian-like AS alteration events including skipped exons (SE), alternative 5′ splice site (A5SS), alternative 3′ splice site (A3SS), mutually exclusive exons (MXE), and retained introns (RI) between genotypes (Fig. 11*A*). We identified a total of 698 and 517 significant splicing defects between APP versus wild-type and APP;Tip60 versus APP comparisons, respectively, that affected every AS event category, suggesting genotype-dependent splicing modifications at a global level (Fig. 11*B*). Although MXE accounts for most significant AS alterations, ∼80% of these alterations are present in Dscam1 gene that encodes for 38,106 distinct proteins via AS of 95 variable exons (Graveley, 2005). Strikingly, a comparison of RNAs showing altered splicing in APP or APP;Tip60 with Tip60 wild-type RNA targets identified from RNA-IP Sequencing data reveal that >50% of RNA undergoing significant AS alterations in APP (186/358) and APP;Tip60 (162/284) brains are bona-fide Tip60-RNA targets in the wild-type brain (Fig. 11*C*). Moreover, ∼30% of human orthologues for these Tip60-targeted AS genes in APP (54/177) and APP;Tip60 (44/152) were found to be enriched for AD in the DisGeNET curated database of gene-disease associations (Piñero et al., 2016; Tables 3, 4). Therefore, our results strongly suggest that Tip60 possesses the ability to influence AS decisions of unspliced pre-mRNA targets implicated in AD pathogenesis.

We next investigated whether restoring Tip60 levels in APP;Tip60 is sufficient to protect against AD-associated AS defects observed in *Drosophila* APP neurodegeneration. To test this, we screened the 54 Tip60-targeted AD-associated AS defects in APP for reversal in APP;Tip60 such that $(\Delta PSI)_{APPTip60} \cong (\Delta PSI)_{APP}$ at the same or a nearby genomic location. Remarkably, we identified 15 triaged Tip60-rescued AS events mapping to 12 genes that are altered in APP and rescued by restoration of Tip60 levels in APP;Tip60 (Table 5). Only 1 out of the 34 MXE events in *Dscam1* gene were included in the main list to avoid repetition (Table 6). These triaged Tip60-rescued AS events are distributed over all five types of AS and have no preference toward exon inclusion or exclusion, suggesting Tip60 is acting as a global splicing regulator (Fig. 12*A*). Individual schematic representations show splicing defects for each AS type that is reversed at the exact exonic/intronic genomic locations (Fig. 12*B*). For example, exon 6 in the *heph* gene is preferentially included in wild-type (PSI = 0.81), skipped in APP (PSI = 0.39), and included back again in APP;Tip60 (PSI= 0.69). Similarly, long isoforms of *Dlg1* exon 1 (A5SS) and *Rab3-GEF* exon 4 (A3SS) are favored in wild-type (PSI= 0.96; 0.44), relatively excluded in APP (PSI = 0.71; 0.00) and restored in APP;Tip60 (PSI = 1.00; 0.34). Likewise, *Dscam1* gene contains mutually exclusive exons at position 6 where a specific exon in wild-type (PSI = 0.88) is skipped for another exon in APP (PSI= 0.05) but included again in APP;Tip60 (PSI = 0.67). Lastly, the intron between exons 3 and 4 in *Adar* gene is less included in wild-type (PSI = 0.77) as compared with APP (PSI= 0.96) that is restored in APP;Tip60 (PSI = 0.60). Finally, to test whether the AS defects we observed in the APP neurodegenerative fly brain are modulated by Tip60-RNA targeting, we used splice-specific RT-qPCR on larval brains from wild-type and RNAi-mediated Tip60 neural knock-down samples (Fig. 12*C–E*). Remarkably, the expression of predominant RNA isoform for *heph* ($t_{(4)}$ = 6.797, p = 0.0012, unpaired Student's t test),

Table 3. Mammalian conservation of Tip60-RNA targets with altered splicing in *Drosophila* APP and APP;Tip60 models

Fly gene ID	Fly symbol	Human gene ID	Human symbol	Ensembl ID	DIOPT score
(A) Mammalian conservation of genes with altered splicing in APP vs wild type					
2768716	Mim	9788	MTSS1	ENSG00000170873	7
2768852	par-1	4140	MARK3	ENSG00000075413	12
30975	Ewg	4899	NRF1	ENSG00000106459	11
31017	Sdk	54549	SDK2	ENSG00000069188	11
31121	CG32809	56243	KIAA1217	ENSG00000120549	9
31130	Adar	104	ADARB1	ENSG00000197381	12
31353	CG43689	23040	MYT1L	ENSG00000186487	7
31364	Fas2	4685	NCAM2	ENSG00000154654	11
31379	Bi	6909	TBX2	ENSG00000121068	11
31425	Ptp4E	5787	PTPRB	ENSG00000127329	12
31429	Ovo	5017	OVOL1	ENSG00000172818	8
31550	Ca-α1T	8911	CACNA1I	ENSG00000100346	11
31722	fs(1)h	6046	BRD2	ENSG00000204256	9
318206	Tlk	11011	TLK2	ENSG00000146872	11
318824	Dpy	2201	FBN2	ENSG00000138829	4
32083	dlg1	1739	DLG1	ENSG00000075711	13
32115	Ptp10D	5787	PTPRB	ENSG00000127329	11
32217	Tomosyn	134957	STXBP5	ENSG00000164506	14
32256	Hep	5609	MAP2K7	ENSG00000076984	12
32273	Sno	55206	SBNO1	ENSG00000139697	13
32278	HDAC4	9759	HDAC4	ENSG00000068024	11
32406	Rut	107	ADCY1	ENSG00000164742	12
32442	Rab3-GEF	8567	MADD	ENSG00000110514	15
32536	Sd	7003	TEAD1	ENSG00000187079	13
32543	Myb	4603	MYBL1	ENSG00000185697	11
32547	Tay	26053	AUTS2	ENSG00000158321	4
32561	Mmd	4185	ADAM11	ENSG00000073670	9
32569	Vap	5921	RASA1	ENSG00000145715	13
32589	CG3632	9110	MTMR4	ENSG00000108389	13
32619	Para	6334	SCN8A	ENSG00000196876	12
32941	CoRest	23186	RCOR1	ENSG00000089902	11
33156	l(2)gl	3996	LLGL1	ENSG00000131899	15
33262	Dock	4690	NCK1	ENSG00000158092	14
33807	CG9171	11041	B4GAT1	ENSG00000174684	7
33923	CG11319	57628	DPP10	ENSG00000175497	9
33989	Caper	9584	RBM39	ENSG00000131051	11
34096	Cka	29966	STRN3	ENSG00000196792	15
34112	Piezo	63895	PIEZO2	ENSG00000154864	13
34127	Pvr	3791	KDR	ENSG00000128052	10
34519	SCAR	10810	WASF3	ENSG00000132970	13
34686	MRP	8714	ABCC3	ENSG00000108846	14
34772	Kuz	102	ADAM10	ENSG00000137845	14
34831	Dyrk2	8798	DYRK4	ENSG00000010219	12
34844	elB	80139	ZNF703	ENSG00000183779	9
35042	CLIP-190	6249	CLIP1	ENSG00000130779	12
35071	CadN2	1002	CDH4	ENSG00000179242	2
35077	Rdo	79883	PODNL1	ENSG00000132000	1
35090	CG42750	64174	DPEP2	ENSG00000167261	8
35107	Pde11	8654	PDE5A	ENSG00000138735	11
35213	CG17544	8310	ACOX3	ENSG00000087008	10
35340	Dia	1730	DIAPH2	ENSG00000147202	14
35359	Sky	57465	TBC1D24	ENSG00000162065	14
35376	Nhe2	6553	SLC9A5	ENSG00000135740	12
35400	CG8671	399665	FAM102A	ENSG00000167106	13
35402	Mondo	22877	MLXIP	ENSG00000175727	13
35420	Cul2	8453	CUL2	ENSG00000108094	14
35442	CG42748	389813	AJM1	ENSG00000232434	6
35524	Src42A	2444	FRK	ENSG00000111816	14
35539	Ars2	51593	SRRT	ENSG00000087087	14
35540	EcR	10062	NR1H3	ENSG00000025434	10
35652	Dscam1	57453	DSCAML1	ENSG00000177103	13
35693	Vps13	23230	VPS13A	ENSG00000197969	13
35771	Lig	55833	UBAP2	ENSG00000137073	11

(*Table continues*.)

Table 3. Continued

Fly gene ID	Fly symbol	Human gene ID	Human symbol	Ensembl ID	DIOPT score
35846	Cirl	22859	ADGRL1	ENSG00000072071	10
35950	Pkn	5586	PKN2	ENSG00000065243	13
35977	Brp	26059	ERC2	ENSG00000187672	7
36121	CG11883	4907	NT5E	ENSG00000135318	2
36176	Metro	143098	MPP7	ENSG00000150054	13
36475	Dh31-R	10203	CALCRL	ENSG00000064989	14
36542	Shot	667	DST	ENSG00000151914	11
36554	RN-tre	9712	USP6NL	ENSG00000148429	11
36689	CG8079	55109	AGGF1	ENSG00000164252	13
36718	Khc-73	63971	KIF13A	ENSG00000137177	13
36753	Strn-Mlck	4638	MYLK	ENSG00000065534	4
36889	Psi	8880	FUBP1	ENSG00000162613	11
36924	CG30460	51101	ZC2HC1A	ENSG00000104427	4
36978	Patronin	23271	CAMSAP2	ENSG00000118200	13
37038	Grh	29841	GRHL1	ENSG00000134317	8
37129	CG43066	55117	SLC6A15	ENSG00000072041	10
37152	Sik3	23387	SIK3	ENSG00000160584	3
37165	Mctp	79772	MCTP1	ENSG00000175471	13
37230	Hts	118	ADD1	ENSG00000087274	14
37254	Sm	3191	HNRNPL	ENSG00000104824	12
37422	ASPP	23368	PPP1R13B	ENSG00000088808	14
37552	Liprin-γ	23254	KAZN	ENSG00000189337	13
37614	CG42260	1260	CNGA2	ENSG00000183862	4
37641	Nahoda	114928	GPRASP2	ENSG00000158301	1
3771968	Msp300	23345	SYNE1	ENSG00000131018	5
3772382	Plp	5116	PCNT	ENSG00000160299	6
37892	mAChR-A	1133	CHRM5	ENSG00000184984	11
37981	NaCP60E	6334	SCN8A	ENSG00000196876	4
38027	Rno	9767	JADE3	ENSG00000102221	10
38142	CG32333	57579	FAM135A	ENSG00000082269	13
38175	Psa	9520	NPEPPS	ENSG00000141279	15
38176	Iml1	9681	DEPDC5	ENSG00000100150	13
38257	mu2	9656	MDC1	ENSG00000137337	4
38327	MEP-1	5326	PLAGL2	ENSG00000126003	1
38344	Atg2	55102	ATG2B	ENSG00000066739	14
38427	Armi	54456	MOV10L1	ENSG00000073146	10
38438	CG32264	221692	PHACTR1	ENSG00000112137	8
38487	CG14995	755	CFAP410	ENSG00000160226	12
38491	Ens	9053	MAP7	ENSG00000135525	4
38578	RhoGEF64C	50650	ARHGEF3	ENSG00000163947	3
38755	Tow	81563	C1orf21	ENSG00000116667	2
38844	CG7546	7917	BAG6	ENSG00000204463	13
38863	Ank2	287	ANK2	ENSG00000145362	6
39004	Fhos	80206	FHOD3	ENSG00000134775	8
39054	Rdl	2568	GABRP	ENSG00000094755	4
39089	MTF-1	4520	MTF1	ENSG00000188786	7
39180	dpr10	1826	DSCAM	ENSG00000171587	1
39198	Rbfox1	54715	RBFOX1	ENSG00000078328	9
39258	IRSp53	10458	BAIAP2	ENSG00000175866	10
39399	App	79683	ZDHHC14	ENSG00000175048	10
39765	Taf4	6875	TAF4B	ENSG00000141384	10
39900	Exn	25791	NGEF	ENSG00000066248	5
39902	CG3764	57600	FNIP2	ENSG00000052795	12
39999	Eip75B	5468	PPARG	ENSG00000132170	4
40146	Tey	55182	RNF220	ENSG00000187147	2
40167	Papss	9061	PAPSS1	ENSG00000138801	14
40292	Pitslre	984	CDK11B	ENSG00000248333	11
40414	CG11247	7652	ZNF99	ENSG00000213973	2
40461	Srpk79D	26576	SRPK3	ENSG00000184343	9
40567	CG31522	79993	ELOVL7	ENSG00000164181	14
40850	Alh	4302	MLLT6	ENSG00000275023	7
40924	CG2993	91947	ARRDC4	ENSG00000140450	6
40928	CG17816	56890	MDM1	ENSG00000111554	1
40933	EMC1	23065	EMC1	ENSG00000127463	13

(*Table continues*.)

Table 3. Continued

Fly gene ID	Fly symbol	Human gene ID	Human symbol	Ensembl ID	DIOPT score
41062	Pyd	9414	TJP2	ENSG00000119139	13
41118	FER	2241	FER	ENSG00000151422	12
41145	Mura	152006	RNF38	ENSG00000137075	7
41749	cv-c	10395	DLC1	ENSG00000164741	9
41771	CG14853	285141	ERICH2	ENSG00000204334	6
41817	CG42788	9758	FRMPD4	ENSG00000169933	9
41911	nsl1	284058	KANSL1	ENSG00000120071	9
42127	Alt	6238	RRBP1	ENSG00000125844	3
42310	unc79	57578	UNC79	ENSG00000133958	14
42327	Dys	1756	DMD	ENSG00000198947	11
42350	GluClα	2741	GLRA1	ENSG00000145888	12
42358	Ire1	10595	ERN2	ENSG00000134398	13
42491	Cortactin	2017	CTTN	ENSG00000085733	13
42600	CG42390	8498	RANBP3	ENSG00000031823	1
42608	CG34377	389432	SAMD5	ENSG00000203727	6
42646	Nrx-1	9378	NRXN1	ENSG00000179915	12
42676	Wake	162282	ANKFN1	ENSG00000153930	10
42687	Wge	84629	TNRC18	ENSG00000182095	7
42742	Irk1	3759	KCNJ2	ENSG00000123700	9
42840	CG13604	84959	UBASH3B	ENSG00000154127	14
42848	Rox8	7073	TIAL1	ENSG00000151923	14
42935	Puf	9736	USP34	ENSG00000115464	14
42940	Slo	3778	KCNMA1	ENSG00000156113	13
43087	Msi	124540	MSI2	ENSG00000153944	5
43277	CG31064	55680	RUFY2	ENSG00000204130	13
43673	Dco	1453	CSNK1D	ENSG00000141551	11
43788	Hcf	29915	HCFC2	ENSG00000111727	9
43795	zfh2	79776	ZFHX4	ENSG00000091656	12
43803	Eph	2047	EPHB1	ENSG00000154928	13
43810	CG11360	51320	MEX3C	ENSG00000176624	11
43841	unc-13	23025	UNC13A	ENSG00000130477	10
44030	msn	23043	TNIK	ENSG00000154310	13
44100	Patj	10207	PATJ	ENSG00000132849	9
44448	Scrib	23513	SCRIB	ENSG00000180900	7
44817	For	5592	PRKG1	ENSG00000185532	13
44885	Mys	3688	ITGB1	ENSG00000150093	14
45248	Nckx30C	25769	SLC24A2	ENSG00000155886	14
45320	Troll	3339	HSPG2	ENSG00000142798	11
45775	mei-P26	81844	TRIM56	ENSG00000169871	4
45840	Cpo	11030	RBPMS	ENSG00000157110	9
45884	Kkv	3036	HAS1	ENSG00000105509	4
47249	Woc	9202	ZMYM4	ENSG00000146463	10
48571	Heph	5725	PTBP1	ENSG00000011304	13
49070	Mbs	4660	PPP1R12B	ENSG00000077157	13
49090	RyR	6262	RYR2	ENSG00000198626	14
5740528	CG34354	7072	TIA1	ENSG00000116001	7
64875	disco-r	646	BNC1	ENSG00000169594	9
64877	Cpx	10815	CPLX1	ENSG00000168993	9
7354466	CG42342	1305	COL13A1	ENSG00000197467	3
8674055	Mgl	4036	LRP2	ENSG00000081479	11
(B) Mammalian conservation of genes with altered splicing in APP;Tip60 vs APP					
14462845	CG43783	55852	TEX2	ENSG00000136478	7
2768685	Mld	51427	ZNF107	ENSG00000196247	2
2768852	par-1	4140	MARK3	ENSG00000075413	12
31004	CG13366	23384	SPECC1L	ENSG00000100014	11
31017	Sdk	54549	SDK2	ENSG00000069188	11
31121	CG32809	56243	KIAA1217	ENSG00000120549	9
31130	Adar	104	ADARB1	ENSG00000197381	12
31169	CG4313	53831	GPR84	ENSG00000139572	5
31309	Dnc	5142	PDE4B	ENSG00000184588	12
31429	Ovo	5017	OVOL1	ENSG00000172818	8
31496	IntS6	203522	INTS6L	ENSG00000165359	12
31722	fs(1)h	6046	BRD2	ENSG00000204256	9

(*Table continues*.)

Table 3. Continued

Fly gene ID	Fly symbol	Human gene ID	Human symbol	Ensembl ID	DIOPT score
31798	CG12065	7378	UPP1	ENSG00000183696	1
31826	rdgA	8525	DGKZ	ENSG00000149091	14
31839	CG7766	5256	PHKA2	ENSG00000044446	13
318930	NimA	375033	PEAR1	ENSG00000187800	4
31957	α-Man-Ia	10905	MAN1A2	ENSG00000198162	13
31991	CG43347	79177	ZNF576	ENSG00000124444	1
32083	dlg1	1739	DLG1	ENSG00000075711	13
32115	Ptp10D	5787	PTPRB	ENSG00000127329	11
32245	Fne	1993	ELAVL2	ENSG00000107105	14
32256	Hep	5609	MAP2K7	ENSG00000076984	12
32278	HDAC4	9759	HDAC4	ENSG00000068024	11
32343	inaE	747	DAGLA	ENSG00000134780	13
32442	Rab3-GEF	8567	MADD	ENSG00000110514	15
32461	HDAC6	10013	HDAC6	ENSG00000094631	14
32536	Sd	7003	TEAD1	ENSG00000187079	13
32544	Gβ13F	2782	GNB1	ENSG00000078369	15
32589	CG3632	9110	MTMR4	ENSG00000108389	13
326128	Ada2a	6871	TADA2A	ENSG00000276234	12
32619	Para	6334	SCN8A	ENSG00000196876	12
326215	SMC5	23137	SMC5	ENSG00000198887	12
32771	Mnb	1859	DYRK1A	ENSG00000157540	10
32930	kek5	340745	LRIT2	ENSG00000204033	2
33002	Nup205	23165	NUP205	ENSG00000155561	13
33048	RhoGAP19D	57636	ARHGAP23	ENSG00000275832	8
33137	l(1)G0196	23262	PPIP5K2	ENSG00000145725	13
33156	l(2)gl	3996	LLGL1	ENSG00000131899	15
33158	Cda5	1486	CTBS	ENSG00000117151	1
33204	Plc21C	23236	PLCB1	ENSG00000182621	13
33392	Aop	2120	ETV6	ENSG00000139083	10
3346235	scaf6	10523	CHERP	ENSG00000085872	12
3346237	Nab	4664	NAB1	ENSG00000138386	11
33690	Smog	57512	GPR158	ENSG00000151025	7
33807	CG9171	11041	B4GAT1	ENSG00000174684	7
33928	CG31635	284352	PPP1R37	ENSG00000104866	8
34030	Ziz	23348	DOCK9	ENSG00000088387	12
34038	Slob	54899	PXK	ENSG00000168297	4
34112	Piezo	63895	PIEZO2	ENSG00000154864	13
34327	CG5850	55751	TMEM184C	ENSG00000164168	13
34686	MRP	8714	ABCC3	ENSG00000108846	14
34701	CG9932	58499	ZNF462	ENSG00000148143	3
34831	Dyrk2	8798	DYRK4	ENSG00000010219	12
34888	Stc	4799	NFX1	ENSG00000086102	14
34950	Ca-α1D	776	CACNA1D	ENSG00000157388	13
34982	Dac	1602	DACH1	ENSG00000276644	12
35042	CLIP-190	6249	CLIP1	ENSG00000130779	12
35047	Dl	5970	RELA	ENSG00000173039	9
35077	Rdo	79883	PODNL1	ENSG00000132000	1
35107	Pde11	8654	PDE5A	ENSG00000138735	11
35109	CG15160	23248	RPRD2	ENSG00000163125	11
35173	Can	22985	ACIN1	ENSG00000100813	10
35340	Dia	1730	DIAPH2	ENSG00000147202	14
35376	Nhe2	6553	SLC9A5	ENSG00000135740	12
35402	Mondo	22877	MLXIP	ENSG00000175727	13
35408	nrv3	481	ATP1B1	ENSG00000143153	14
35652	Dscam1	57453	DSCAML1	ENSG00000177103	13
35715	LRR	55604	CARMIL1	ENSG00000079691	15
35900	Babo	7046	TGFBR1	ENSG00000106799	14
35950	Pkn	5586	PKN2	ENSG00000065243	13
36084	CAP	10174	SORBS3	ENSG00000120896	7
36527	fl(2)d	9589	WTAP	ENSG00000146457	11
36658	Pcf.11	51585	PCF11	ENSG00000165494	11
36753	Strn-Mlck	4638	MYLK	ENSG00000065534	4
36978	Patronin	23271	CAMSAP2	ENSG00000118200	13
37038	Grh	29841	GRHL1	ENSG00000134317	8

(*Table continues*.)

Table 3. Continued

Fly gene ID	Fly symbol	Human gene ID	Human symbol	Ensembl ID	DIOPT score
37152	Sik3	23387	SIK3	ENSG00000160584	3
37199	CG15118	338692	ANKRD13D	ENSG00000172932	14
37254	Sm	3191	HNRNPL	ENSG00000104824	12
37288	Ate1	11101	ATE1	ENSG00000107669	14
37528	Fmr1	8087	FXR1	ENSG00000114416	12
3772382	Plp	5116	PCNT	ENSG00000160299	6
37979	NKAIN	154215	NKAIN2	ENSG00000188580	9
38063	CG1233	79894	ZNF672	ENSG00000171161	1
38173	Hfp	22827	PUF60	ENSG00000179950	14
38257	mu2	9656	MDC1	ENSG00000137337	4
38327	MEP-1	5326	PLAGL2	ENSG00000126003	1
38427	Armi	54456	MOV10L1	ENSG00000073146	10
38963	Unr	7812	CSDE1	ENSG00000009307	15
39198	Rbfox1	54715	RBFOX1	ENSG00000078328	9
39258	IRSp53	10458	BAIAP2	ENSG00000175866	10
39262	GlcAT-P	27087	B3GAT1	ENSG00000109956	4
39533	Dysc	25861	WHRN	ENSG00000095397	11
39744	Brm	6595	SMARCA2	ENSG00000080503	13
39902	CG3764	57600	FNIP2	ENSG00000052795	12
39919	Rbp6	124540	MSI2	ENSG00000153944	13
40167	Papss	9061	PAPSS1	ENSG00000138801	14
40171	Su(Tpl)	22936	ELL2	ENSG00000118985	10
40220	CG17233	79780	CCDC82	ENSG00000149231	5
40433	Nopp140	9221	NOLC1	ENSG00000166197	3
40461	Srpk79D	26576	SRPK3	ENSG00000184343	9
40515	Nrm	84033	OBSCN	ENSG00000154358	1
40560	CG32944	55351	STK32B	ENSG00000152953	13
40567	CG31522	79993	ELOVL7	ENSG00000164181	14
40793	Gpp	84444	DOT1L	ENSG00000104885	12
40928	CG17816	56890	MDM1	ENSG00000111554	1
41145	Mura	152006	RNF38	ENSG00000137075	7
41225	Mical	9645	MICAL2	ENSG00000133816	8
41592	CG31342	6386	SDCBP	ENSG00000137575	4
41612	Sim	6492	SIM1	ENSG00000112246	9
41737	Trx	9757	KMT2B	ENSG00000272333	9
41817	CG42788	9758	FRMPD4	ENSG00000169933	9
41911	nsl1	284058	KANSL1	ENSG00000120071	9
42150	Rim	22999	RIMS1	ENSG00000079841	10
42413	CG4360	7637	ZNF84	ENSG00000198040	1
42601	SKIP	54440	SASH3	ENSG00000122122	6
42687	Wge	84629	TNRC18	ENSG00000182095	7
42824	Sba	55777	MBD5	ENSG00000204406	7
42845	Miro	55288	RHOT1	ENSG00000126858	14
42854	Syx1A	6804	STX1A	ENSG00000106089	15
42935	Puf	9736	USP34	ENSG00000115464	14
43105	LpR2	7436	VLDLR	ENSG00000147852	12
43126	CG5890	30820	KCNIP1	ENSG00000182132	13
43130	Lnk	10603	SH2B2	ENSG00000160999	11
43317	Tusp	56995	TULP4	ENSG00000130338	13
43399	CG1646	55015	PRPF39	ENSG00000185246	10
43469	Ptp99A	5793	PTPRG	ENSG00000144724	9
43505	Wdr24	84219	WDR24	ENSG00000127580	14
43535	CG31038	23625	FAM89B	ENSG00000176973	2
43710	PNPase	87178	PNPT1	ENSG00000138035	15
43788	Hcf	29915	HCFC2	ENSG00000111727	9
43809	Slip1	23024	PDZRN3	ENSG00000121440	11
43856	Nej	2033	EP300	ENSG00000100393	12
43923	Axo	26047	CNTNAP2	ENSG00000174469	5
43924	Jim	10794	ZNF460	ENSG00000197714	2
43997	Jbug	2316	FLNA	ENSG00000196924	3
44018	Cas	54897	CASZ1	ENSG00000130940	7
44039	Pak	5058	PAK1	ENSG00000149269	14
44160	Sw	1781	DYNC1I2	ENSG00000077380	13
44448	Scrib	23513	SCRIB	ENSG00000180900	7

(*Table continues*.)

Table 3. Continued

Fly gene ID	Fly symbol	Human gene ID	Human symbol	Ensembl ID	DIOPT score
44861	Sdt	64398	MPP5	ENSG00000072415	12
45248	Nckx30C	25769	SLC24A2	ENSG00000155886	14
45320	Troll	3339	HSPG2	ENSG00000142798	11
45380	Spin	83985	SPNS1	ENSG00000169682	13
46194	Spn	55607	PPP1R9A	ENSG00000158528	11
48571	Heph	5725	PTBP1	ENSG00000011304	13
48973	Src64B	6714	SRC	ENSG00000197122	9
49070	Mbs	4660	PPP1R12B	ENSG00000077157	13
49968	Cadps	8618	CADPS	ENSG00000163618	14
50225	Prosap	50944	SHANK1	ENSG00000161681	11
7354466	CG42342	1305	COL13A1	ENSG00000197467	3
7354470	CG42402	59271	EVA1C	ENSG00000166979	8

Significantly altered splicing events in (A) APP versus wild type and (B) APP;Tip60 versus APP were mapped to fly genome and filtered for Tip60 RNA targets immunoprecipitated in *Drosophila* wild-type genotype. Conserved human orthologs were predicted using best match from the DRSC integrative ortholog prediction tool (DIOPT). Human ortholog match were found for 177/186 and 152/162 splicing targets in the APP versus wild type and APP;tip60 versus APP comparisons, respectively.

Dscam1 ($t_{(4)}$ = 7.707, p = 0.0008, unpaired Student's t test), and *Adar* ($t_{(4)}$ = 2.530, p = 0.0323, unpaired Student's t test) in the wild-type larval brain was found to be significantly reduced on Tip60 RNAi-mediated knock-down. In conclusion, neural Tip60 knock-down is sufficient for inducing the exact AS defects identified in *heph*, *Dscam1*, and *Adar* under APP neurodegeneration., therefore validating the role of Tip60 in modulating AS decisions of its pre-mRNA targets.

Tip60's RNA-binding function is conserved in the human brain and altered under AD pathology

The human orthologues of the 12 triaged Tip60-rescued AS genes perform diverse yet critical neuronal functions that go awry in AD pathogenesis (Fig. 13*A*). For example, ADAM10 (fly *kuz*) is a α-secretase that cleaves APP to promote the nonamyloidogenic pathway and reduce Aβ plaque load (Niemitz, 2013; Yuan et al., 2017). Accordingly, ADAM10 is the third most significant AD-associated gene in DisGeNET database (Piñero et al., 2016) and is currently being tested as a potential AD treatment (Manzine et al., 2019). Likewise, DLG1 (fly *dlg1*) is a scaffolding protein known to interact with APP intracellular C-terminal domain (AICD; Silva et al., 2020) and regulate APP metabolism by recruiting ADAM10 to the synapse (Marcello et al., 2013). Additionally, RBFOX1 (fly *Rbfox1*) and PTBP1 (fly *heph*) are two key splicing regulators of neuronal-specific AS in the mammalian brain (D. Li et al., 2021) that directly regulate AS of APP exon 7 (Smith et al., 2011; Alam et al., 2014) and therefore, control APP^{695} production and Aβ plaque load (Belyaev et al., 2010). Similarly, ADARB1 (fly *Adar*) is a major adenosine to inosine RNA editing enzyme in mammals that also regulates splicing (Solomon et al., 2013) and its function is reduced in human AD hippocampus (Khermesh et al., 2016; Annese et al., 2018). Moreover, HSPG2 (fly *trol*) extracellular matrix protein is observed to be co-deposited with Aβ plaques in the brains of AD patients (Van Gool et al., 1993; G.L. Zhang et al., 2014) where it accelerates Aβ oligomerization and aggregation (C.C. Liu et al., 2016). Besides, MADD (fly *Rab3-GEF*) and HDAC4 show altered expression in AD pathology (Del Villar and Miller, 2004; X. Shen et al., 2016) and have been proposed to serve as novel AD pharmacological targets (Mielcarek et al., 2015; Hassan et al., 2021).

Importantly, and consistent with our data, several studies have previously reported AS defects in postmortem human AD-brains in 7 out of these 12 triaged Tip60-rescued AS genes (Tollervey et al., 2011; Raj et al., 2018; Adusumalli et al., 2019; Marques-Coelho et al., 2021). To test whether Tip60's RNA binding function is conserved in the human brain and whether such putative Tip60-RNA binding is altered under human AD pathology, we performed RIP-qPCR on RNA isolated from postmortem human hippocampal tissues obtained from healthy controls and AD patients (Fig. 13*B*). Remarkably, we found that Tip60 interacted with RNAs corresponding to the seven human Tip60-rescued AS *Drosophila* orthologs that exhibit known AS defects in the human AD brain. Importantly, as compared with healthy controls, Tip60 enrichment for RNA transcripts encoded by each of these 7 loci was significantly reduced in AD patients ($F_{(7,32)}$ = 3.775, p = 0.0043, two-way ANOVA with Sidak's multiple comparison test). Notably, Tip60 enrichment for ADAM10 transcripts in the healthy brain is most significantly reduced in AD brain ($t_{(32)}$ = 5.756, p = 1.10045E-06), supporting a role for Tip60 in mediating RNA processing of genes critical for keeping AD neurodegeneration in check. Together, our results reveal a novel RNA splicing regulatory function for Tip60 that mediates AS decisions for its unspliced pre-mRNA targets enriched for AS impairments that hallmark AD etiology.

Discussion

The selective interaction of Tip60 with protein coding neural mRNAs is disrupted in AD brain

Tip60, the second most highly expressed HAT in the mammalian brain, drives neural function and neuroprotection in AD but studies to date have conventionally focused on its role in chromatin dynamics and neural gene control, leaving additional mechanistic functions unexplored. Here, we report a highly specific, selective, and reproducible RNA-binding function for Tip60's chromodomain in the *Drosophila* brain *in vivo*. Our findings are not unprecedented as chromodomains within multiple chromatin regulatory proteins have been shown to directly interact with RNA (Akhtar et al., 2000; Morales et al., 2005; Bernstein et al., 2006; Shimojo et al., 2008; Ishida et al., 2012; Akoury et al., 2019). Chromodomains within MOF HAT and chromobox-7 achieve dosage compensation by targeting roX noncoding RNA at the male X chromosome and *Xist* noncoding RNA at the female X chromosome in *Drosophila* and mammalian cells, respectively (Akhtar et al., 2000; Bernstein et al., 2006). Our findings confirm and extend these studies by being the first to sequence and characterize a complex array of neural RNAs that are specifically bound to Tip60 in the fly brain. We find that Tip60 primarily targets protein encoding RNAs that mediate dynamic neuronal processes and are enriched for human diseases

Table 4. Tip60-RNA Targets with altered splicing enriched in DisGeNET Alzheimer's disease database

No.	Fly gene ID	Fly symbol	Human symbol	Human gene ID	Gene full name
(A) Alzheimer's disease enrichment for genes with altered splicing in APP vs wild type					
1	2768852	par-1	MARK3	4140	Microtubule affinity regulating kinase 3
2	30975	Ewg	NRF1	4899	Nuclear respiratory factor 1
3	31121	CG32809	KIAA1217	56243	KIAA1217
4	31130	Adar	ADARB1	104	Adenosine deaminase RNA-specific B1
5	31353	CG43689	ST18	9705	ST18 C2H2C-type zinc finger transcription factor
6	31364	Fas2	NCAM2	4685	Neural cell adhesion molecule 2
7	31379	bi	TBX2	6909	T-box transcription factor 2
8	31722	fs(1)h	BRD2	6046	Bromodomain containing 2
9	32083	dlg1	DLG1	1739	Discs large MAGUK scaffold protein 1
10	32273	sno	SBNO1	55206	Strawberry notch homolog 1
11	32278	HDAC4	HDAC4	9759	Histone deacetylase 4
12	32442	Rab3-GEF	MADD	8567	MAP kinase activating death domain
13	32569	vap	RASA1	5921	RAS p21 protein activator 1
14	32941	CoRest	RCOR1	23186	REST corepressor 1
15	34127	Pvr	KDR	3791	Kinase insert domain receptor
16	34519	SCAR	WASF3	10810	WASP family member 3
17	34772	kuz	ADAM10	102	ADAM metallopeptidase domain 10
18	35071	CadN2	CDH1	999	Cadherin 1
19	35077	rdo	IGFALS	3483	Insulin like growth factor binding protein acid labile subunit
20	35090	CG42750	DPEP2	64174	Dipeptidase 2
21	35107	Pde11	PDE5A	8654	Phosphodiesterase 5A
22	35524	Src42A	FRK	2444	fyn-related Src family tyrosine kinase
23	35540	EcR	NR1H3	10062	Nuclear receptor subfamily 1 group H member 3
24	35652	Dscam1	DSCAML1	57453	DS cell adhesion molecule like 1
25	36121	CG11883	NT5E	4907	5′-nucleotidase ecto
26	36542	shot	DST	667	Dystonin
27	37129	CG43066	SLC6A15	55117	Solute carrier family 6 member 15
28	37552	Liprin-γ	KAZN	23254	Kazrin, periplakin interacting protein
29	37641	nahoda	GPRASP2	114928	G-protein-coupled receptor associated sorting protein 2
30	3771968	Msp300	SYNE1	23345	Spectrin repeat containing nuclear envelope protein 1
31	37892	mAChR-A	CHRM1	1128	Cholinergic receptor muscarinic 1
32	38175	Psa	NPEPPS	9520	Aminopeptidase puromycin sensitive
33	38487	CG14995	CFAP410	755	Cilia and flagella associated protein 410
34	39198	Rbfox1	RBFOX1	54715	RNA binding fox-1 homolog 1
35	39999	Eip75B	PPARG	5468	Peroxisome proliferator activated receptor γ
36	40924	CG2993	TXNIP	10628	Thioredoxin interacting protein
37	42327	Dys	DMD	1756	Dystrophin
38	42491	Cortactin	CTTN	2017	Cortactin
39	42646	Nrx-1	NRXN1	9378	Neurexin 1
40	42840	CG13604	UBASH3B	84959	Ubiquitin associated and SH3 domain containing B
41	42940	slo	KCNMA1	3778	Potassium calcium-activated channel subfamily M α 1
42	43087	msi	MSI2	124540	Musashi RNA binding protein 2
43	43673	dco	CSNK1D	1453	Casein kinase 1 δ
44	43795	zfh2	ZFHX3	463	Zinc finger homeobox 3
45	44885	mys	ITGB1	3688	Integrin subunit β 1
46	45248	Nckx30C	SLC24A2	25769	Solute carrier family 24 member 2
47	45320	trol	HSPG2	3339	Heparan sulfate proteoglycan 2
48	45884	kkv	HAS1	3036	Hyaluronan synthase 1
49	48571	heph	PTBP1	5725	Polypyrimidine tract binding protein 1
50	49090	RyR	RYR2	6262	Ryanodine receptor 2
51	5740528	CG34354	TIA1	7072	TIA1 cytotoxic granule associated RNA binding protein
52	64875	disco-r	BNC1	54796	Basonuclin 1
53	64877	cpx	CPLX1	10815	Complexin 1
54	8674055	mgl	LRP2	4036	LDL receptor-related protein 2
(B) Alzheimer's disease enrichment for genes with altered splicing in APP;Tip60 vs APP					
1	2768852	par-1	MARK3	4140	Microtubule affinity regulating kinase 3
2	31121	CG32809	KIAA1217	56243	KIAA1217
3	31130	Adar	ADARB1	104	Adenosine deaminase RNA-specific B1
4	31722	fs(1)h	BRD2	6046	Bromodomain containing 2
5	31826	rdgA	DGKZ	8525	Diacylglycerol kinase zeta
6	32083	dlg1	DLG1	1739	Discs large MAGUK scaffold protein 1
7	32245	fne	ELAVL2	1993	ELAV like RNA binding protein 2

(*Table continues*.)

Table 4. Continued

No.	Fly gene ID	Fly symbol	Human symbol	Human gene ID	Gene full name
8	32278	HDAC4	HDAC4	9759	Histone deacetylase 4
9	32442	Rab3-GEF	MADD	8567	MAP kinase activating death domain
10	32461	HDAC6	HDAC6	10013	Histone deacetylase 6
11	32771	mnb	DYRK1A	1859	Dual specificity tyrosine phosphorylation regulated kinase 1A
12	33158	Cda5	CTBS	1486	Chitobiase
13	33204	Plc21C	PLCB1	23236	Phospholipase C β 1
14	33928	CG31635	PPP1R37	284352	Protein phosphatase 1 regulatory subunit 37
15	35047	dl	RELA	5970	RELA protooncogene, NF-kB subunit
16	35077	rdo	IGFALS	3483	Insulin like growth factor binding protein acid labile subunit
17	35107	Pde11	PDE5A	8654	Phosphodiesterase 5A
18	35652	Dscam1	DSCAML1	57453	DS cell adhesion molecule like 1
19	35900	babo	TGFBR1	7046	Transforming growth factor β receptor 1
20	36084	CAP	SORBS3	10174	Sorbin and SH3 domain containing 3
21	37979	NKAIN	NKAIN2	154215	Sodium/potassium transporting ATPase interacting 2
22	39198	Rbfox1	RBFOX1	54715	RNA binding fox-1 homolog 1
23	39262	GlcAT-P	B3GAT1	27087	β-1,3-glucuronyltransferase 1
24	39919	Rbp6	MSI2	124540	Musashi RNA binding protein 2
25	40433	Nopp140	NOLC1	9221	Nucleolar and coiled-body phosphoprotein 1
26	40515	nrm	SIRPB1	10326	Signal regulatory protein β 1
27	40560	CG32944	STK32B	55351	Serine/threonine kinase 32B
28	41225	Mical	MICAL2	9645	Microtubule associated monooxygenase, calponin and LIM domain containing 2
29	41592	CG31342	SDCBP2	27111	Syndecan binding protein 2
30	41612	sim	SIM2	6493	SIM bHLH transcription factor 2
31	42854	Syx1A	STX1A	6804	Syntaxin 1A
32	43105	LpR2	VLDLR	7436	Very low-density lipoprotein receptor
33	43317	Tusp	TULP4	56995	TUB like protein 4
34	43469	Ptp99A	PTPRG	5793	Protein tyrosine phosphatase receptor type G
35	43856	nej	EP300	2033	E1A binding protein p300
36	43923	axo	CNTNAP2	26047	Contactin associated protein 2
37	43997	jbug	FLNA	2316	Filamin A
38	44018	cas	CASZ1	54897	Castor zinc finger 1
39	44039	Pak	PAK1	5058	p21 (RAC1) activated kinase 1
40	45248	Nckx30C	SLC24A2	25769	Solute carrier family 24 member 2
41	45320	trol	HSPG2	3339	Heparan sulfate proteoglycan 2
42	48571	heph	PTBP1	5725	Polypyrimidine tract binding protein 1
43	48973	Src64B	FYN	2534	FYN protooncogene, Src family tyrosine kinase
44	50225	Prosap	SHANK1	50944	SH3 and multiple ankyrin repeat domains 1

Conserved human orthologs of Tip60-RNA targets with significantly altered splicing events in (A) APP versus wild type and (B) APP;Tip60 versus APP were compared with the curated DisGeNET gene-disease association database for Alzheimer's disease (AD). A total of 54 genes and 44 genes were found to be associated with AD from the APP versus wild-type and APP;Tip60 versus APP splicing comparisons, respectively.

such as tauopathy and AD, indicating disruption of Tip60-RNA binding is involved in these cognitive disorders. In line with these findings, we observe that Tip60-RNA targeting is disrupted in the AD fly brain and in AD human hippocampal samples supporting a functional role for Tip60-RNA binding in AD pathology. Remarkably, increasing Tip60 levels in the AD fly brain partially protects against Tip60-RNA targeting alterations that are enriched for dynamic neuronal processes including chromatin assembly and remodeling, axonal guidance, protein modification processes, and RNA splicing and transport. We speculate that such Tip60-RNA binding disruptions lead to transcriptomic alterations that ultimately contribute significantly to AD pathologies but can be protected against by increased Tip60 levels.

Tip60's bi-level gene regulation at the chromatin and RNA level mediates rapid fine-tuning of neural gene expression

Tip60 is a key mediator of activity-dependent gene expression underlying dynamic neuronal processes and is shuttled from cytoplasm into nucleus on neuronal stimulation for histone acetylation (Xu et al., 2016; Karnay et al., 2019). This raises the possibility that Tip60 could be binding with RNA emanating from its activity-dependent genes at various stages of RNA processing to dictate ultimate protein isoforms and function in the brain. However, whether Tip60 interacts with nascent RNAs in the nucleus or mature RNA in the cytoplasm and whether Tip60's interacting RNAs are transcribed directly from Tip60 chromatin targets remains unclear. Here, we show enrichment of intronic regions in the Tip60-IP bound RNA samples, indicative of Tip60 primarily targeting unspliced pre-mRNAs that reside in the nucleus. Further, we found reduced Tip60 staining on polytene chromosomes after RNase treatment, strongly suggesting that Tip60 interacts with newly transcribed pre-mRNA in close proximity to chromatin. Consistent with this finding, we identified a significant overlap between Tip60's RNA targets and its chromatin gene targets, suggesting Tip60 is regulating expression and function of identical neural targets via targeting at both the chromatin and RNA levels, respectively. Although our findings are unprecedented for a histone acetyltransferase, HP1 chromosomal protein has been shown to dissociate with heterochromatin to bind with newly synthesized RNA owing to its greater affinity for RNA over histones (Keller et al., 2012). In support of this concept, we find Tip60 is unlikely to bind with both histone and RNA concurrently because of steric hindrance at interacting sites. Therefore, we are the first to propose a model by which Tip60 rapidly fine-tunes its neural targets for dynamic gene regulation by orchestrating a bi-level switching mechanism such that Tip60 recruitment to chromatin allows for histone acetylation-mediated gene activation as well as targeting of newly synthesized

Table 5. Genomic coordinates of the triaged Tip60-rescued splicing events from rMATS analysis

(A) Skipped exon (SE)

Genotype comparison	Gene	chr	Strand	Skipped exon	Exon Start	Exon end	Upstream exon start	Upstream exon end	δ PSI
APPvsWT	Adar	chrX	+	3	1778369	1778560	1775698	1775738	−0.238
APPTip60vsAPP	Adar	chrX	+	3	1778369	1778560	1775698	1775738	0.336
APPvsWT	Dscam1	chr2R	−	9	7344663	7344954	7344278	7344569	−0.182
APPTip60vsAPP	Dscam1	chr2R	−	9	7344278	7344569	7332260	7332380	0.229
APPvsWT	heph	chr3R	−	6	31931774	31932614	31921632	31921674	−0.421
APPTip60vsAPP	heph	chr3R	−	6	31931774	31932614	31921632	31921674	0.305
APPvsWT	kuz	chr2L	+	3	13558799	13558832	13551141	13551666	−0.244
APPTip60vsAPP	kuz	chr2L	+	12	13636383	13636843	13635648	13636213	0.089
APPvsWT	trol	chrX	−	20	2495040	2495238	2492987	2493215	0.287
APPTip60vsAPP	trol	chrX	−	20	2495040	2495238	2492987	2493215	−0.11

(B) Alternative 5′ splice site (A5SS)

Genotype comparison	Gene	chr	Strand	A5SS exon position	Long exon start	Long exon end	Short exon start	Short exon end	δ PSI
APPvsWT	dlg1	chrX	+	1	11389667	11389781	11389667	11389697	−0.248
APPTip60vsAPP	dlg1	chrX	+	1	11389667	11389781	11389667	11389697	0.289
APPvsWT	fs(1)h	chrX	−	1	8056316	8056701	8056609	8056701	−0.209
APPTip60vsAPP	fs(1)h	chrX	−	1	8056316	8056701	8056609	8056701	0.154
APPTip60vsAPP	CG32809	chrX	−	1	1692296	1692768	1692438	1692768	−0.29

(C) Alternative 3′ splice site (A3SS)

Genotype comparison	Gene	chr	Strand	A3SS exon position	Long exon start	Long exon end	Short exon start	Short exon end	δ PSI
APPvsWT	CG32809	chrX	−	3	1685186	1685535	1685186	1685279	0.632
APPvsWT	HDAC4	chrX	−	5	13270390	13270693	13270390	13270612	0.242
APPvsWT	Nckx30C	chr2L	−	2	9742374	9744230	9742374	9744226	0.362
APPTip60vsAPP	Nckx30C	chr2L	−	1	9746406	9746495	9746433	9746495	−0.231
APPvsWT	Rab3-GEF	chrX	+	4	15094069	15094613	15094093	15094613	−0.436
APPTip60vsAPP	Rab3-GEF	chrX	+	4	15094069	15094613	15094093	15094613	0.366

(D) Mutually exclusive exons (MXE)

Genotype comparison	Gene	chr	Strand	MXE exon position	1st exon start	1st exon end	2nd exon start	2nd exon end	δ PSI
APPvsWT	Adar	chrX	+	2	1775649	1775738	1778369	1778560	0.634
APPTip60vsAPP	Adar	chrX	+	2	1775649	1775738	1778369	1778560	−0.621
APPvsWT	Dscam1	chr2R	−	6	7357590	7357714	7359441	7359565	−0.83
APPTip60vsAPP	Dscam1	chr2R	−	6	7357590	7357714	7359441	7359565	0.619
APPTip60vsAPP	HDAC4	chrX	−	3	13276434	13276547	13282165	13282229	−0.102
APPvsWT	Rbfox1	chr3L	+	9	10581841	10582118	10584815	10585539	0.198
APPTip60vsAPP	Rbfox1	chr3L	+	3	10568128	10568605	10571048	10571246	−0.108

(E) Retained intron (RI)

Genotype comparison	Gene	chr	Strand	Intron between exons	RI exon start	RI exon end	Upstream exon start	Upstream exon end	δ PSI
APPvsWT	Adar	chrX	+	3 and 4	1778369	1778699	1778369	1778560	0.19
APPTip60vsAPP	Adar	chrX	+	3 and 4	1778369	1778699	1778369	1778560	−0.352

Differential splicing isoforms were quantified as percent spliced in (PSI) using rMATS. Difference in isoform abundance between genotypes APP versus wild type and APP;Tip60 versus APP is reported as δ PSI. Alternative splicing events include: (A) skipped exon (SE), (B) alternative 5′ splice site (A5SS), (C) alternative 3′ splice site (A3SS), (D) mutually exclusive exons (MXE), and (E) retained intron (RI).

RNA that may further stabilize binding in a positive feedback loop (Fig. 14).

Tip60-mediated alternative splicing selection may underly splicing defects characterized as hallmarks of Alzheimer's disease

RNA splicing abnormalities have recently emerged as a widespread hallmark in AD and AS defects in major disease candidate genes, including APP, Tau, PSEN, and ApoE, have since been linked to AD pathology (Love et al., 2015; Jakubauskienė and Kanopka, 2021; D. Li et al., 2021). Although causes remain unclear, dysregulation of epigenetic mechanisms under AD pathology (X. Liu et al., 2018; Nativio et al., 2018) and their recent convergence with co-transcriptional AS regulation (Luco et al., 2011; Rahhal and Seto, 2019; Xu et al., 2021) strongly suggest a causative role for epigenetic regulators/modifications in AS defects underlying AD pathology. In support of this concept, here we show that the Tip60 HAT doubles as an RNA splicing modulator and mediates AS selection of its pre-mRNA targets associated with AD. We discovered a multitude of differential mammalian-like AS alteration events in the APP AD fly brain, with over half of these altered RNAs identified as bona-fide Tip60-RNA targets enriched for AD that are partially protected against by increasing Tip60 levels. Moreover, consistent with a previous finding that shows Tip60 knock-down in epithelial cells alters AS of a key integrin subunit (Bhatia et al., 2020), we find Tip60 neural knock-down is sufficient for inducing AS defects identified under APP neurodegeneration, therefore underscoring criticality of Tip60-mediated AS regulation in AD pathogenesis. Further, since several Tip60-rescued fly AS genes show splicing defects in postmortem AD human brains (Tollervey et al., 2011; Raj et al., 2018; Adusumalli et al., 2019; Marques-Coelho et al., 2021) and we find Tip60-RNA binding

Table 6. Tip60-Rescued mutually exclusive splicing events in *Dscam1*

Genotype comparison	Gene	chr	Strand	MXE exon position	1st exon start	1st exon end	2nd exon start	2nd exon end	δ PSI
APPvsWT	Dscam1	chr2R	—	9	7334387	7334666	7343717	7344008	−0.625
APPTip60vsAPP	Dscam1	chr2R	—	9	7334387	7334666	7343717	7344008	0.292
APPvsWT	Dscam1	chr2R	—	9	7334387	7334666	7334933	7335218	−0.238
APPTip60vsAPP	Dscam1	chr2R	—	9	7334387	7334666	7334933	7335218	0.196
APPvsWT	Dscam1	chr2R	—	9	7334387	7334666	7335715	7336003	−0.218
APPTip60vsAPP	Dscam1	chr2R	—	9	7334387	7334666	7335715	7336003	0.176
APPvsWT	Dscam1	chr2R	—	9	7334933	7335218	7337493	7337781	−0.161
APPTip60vsAPP	Dscam1	chr2R	—	9	7334933	7335218	7337493	7337781	0.353
APPvsWT	Dscam1	chr2R	—	9	7335715	7336003	7337493	7337781	−0.164
APPTip60vsAPP	Dscam1	chr2R	—	9	7335715	7336003	7337493	7337781	0.25
APPvsWT	Dscam1	chr2R	—	9	7337493	7337781	7344278	7344569	0.105
APPTip60vsAPP	Dscam1	chr2R	—	9	7337493	7337781	7344278	7344569	−0.31
APPvsWT	Dscam1	chr2R	—	9	7337493	7337781	7345484	7345775	0.108
APPTip60vsAPP	Dscam1	chr2R	—	9	7337493	7337781	7345484	7345775	−0.347
APPvsWT	Dscam1	chr2R	—	9	7337493	7337781	7342582	7342881	0.265
APPTip60vsAPP	Dscam1	chr2R	—	9	7337493	7337781	7342582	7342881	−0.433
APPvsWT	Dscam1	chr2R	—	9	7337493	7337781	7341327	7341618	0.432
APPTip60vsAPP	Dscam1	chr2R	—	9	7337493	7337781	7341327	7341618	−0.75
APPvsWT	Dscam1	chr2R	—	9	7337493	7337781	7345060	7345351	0.515
APPTip60vsAPP	Dscam1	chr2R	—	9	7337493	7337781	7345060	7345351	−0.75
APPvsWT	Dscam1	chr2R	—	9	7341327	7341618	7341707	7341995	−0.423
APPTip60vsAPP	Dscam1	chr2R	—	9	7341327	7341618	7341707	7341995	0.551
APPvsWT	Dscam1	chr2R	—	9	7341327	7341618	7343717	7344008	−0.361
APPTip60vsAPP	Dscam1	chr2R	—	9	7341327	7341618	7343717	7344008	0.472
APPvsWT	Dscam1	chr2R	—	9	7349787	7349911	7350957	7351081	0.556
APPTip60vsAPP	Dscam1	chr2R	—	9	7349787	7349911	7350957	7351081	−0.222
APPvsWT	Dscam1	chr2R	—	6	7350781	7350905	7359441	7359565	−0.861
APPTip60vsAPP	Dscam1	chr2R	—	6	7350781	7350905	7359441	7359565	0.383
APPvsWT	Dscam1	chr2R	—	6	7352898	7353022	7360081	7360205	−0.667
APPTip60vsAPP	Dscam1	chr2R	—	6	7352898	7353022	7360081	7360205	0.5
APPvsWT	Dscam1	chr2R	—	6	7352898	7353022	7358215	7358339	−0.6
APPTip60vsAPP	Dscam1	chr2R	—	6	7352898	7353022	7358215	7358339	0.378
APPvsWT	Dscam1	chr2R	—	6	7352898	7353022	7353244	7353365	−0.489
APPTip60vsAPP	Dscam1	chr2R	—	6	7352898	7353022	7353244	7353365	0.356
APPvsWT	Dscam1	chr2R	—	6	7353244	7353365	7359441	7359565	−0.374
APPTip60vsAPP	Dscam1	chr2R	—	6	7353244	7353365	7359441	7359565	0.264
APPvsWT	Dscam1	chr2R	—	6	7353244	7353365	7359015	7359139	0.367
APPTip60vsAPP	Dscam1	chr2R	—	6	7353244	7353365	7359015	7359139	−0.389
APPvsWT	Dscam1	chr2R	—	6	7353244	7353365	7356316	7356440	0.474
APPTip60vsAPP	Dscam1	chr2R	—	6	7353244	7353365	7356316	7356440	−0.4
APPvsWT	Dscam1	chr2R	—	6	7353244	7353365	7359221	7359345	0.236
APPTip60vsAPP	Dscam1	chr2R	—	6	7353244	7353365	7359221	7359345	−0.48
APPvsWT	Dscam1	chr2R	—	6	7353244	7353365	7360525	7360649	0.427
APPTip60vsAPP	Dscam1	chr2R	—	6	7353244	7353365	7360525	7360649	−0.5
APPvsWT	Dscam1	chr2R	—	6	7353244	7353365	7357590	7357714	0.688
APPTip60vsAPP	Dscam1	chr2R	—	6	7353244	7353365	7357590	7357714	−0.58
APPvsWT	Dscam1	chr2R	—	6	7354056	7354177	7356316	7356440	0.496
APPTip60vsAPP	Dscam1	chr2R	—	6	7354056	7354177	7356316	7356440	−0.407
APPvsWT	Dscam1	chr2R	—	6	7354881	7355005	7359441	7359565	−0.309
APPTip60vsAPP	Dscam1	chr2R	—	6	7354881	7355005	7359441	7359565	0.333
APPvsWT	Dscam1	chr2R	—	6	7355086	7355210	7359441	7359565	−0.419
APPTip60vsAPP	Dscam1	chr2R	—	6	7355086	7355210	7359441	7359565	0.328
APPvsWT	Dscam1	chr2R	—	6	7355086	7355210	7360525	7360649	0.359
APPTip60vsAPP	Dscam1	chr2R	—	6	7355086	7355210	7360525	7360649	−0.396
APPvsWT	Dscam1	chr2R	—	6	7355086	7355210	7357590	7357714	0.578
APPTip60vsAPP	Dscam1	chr2R	—	6	7355086	7355210	7357590	7357714	−0.467
APPvsWT	Dscam1	chr2R	—	6	7357182	7357306	7357590	7357714	0.523
APPTip60vsAPP	Dscam1	chr2R	—	6	7357182	7357306	7357590	7357714	−0.5
APPvsWT	Dscam1	chr2R	—	6	7357590	7357714	7359441	7359565	−0.83
APPTip60vsAPP	Dscam1	chr2R	—	6	7357590	7357714	7359441	7359565	0.619
APPvsWT	Dscam1	chr2R	—	6	7357590	7357714	7360081	7360205	−0.606
APPTip60vsAPP	Dscam1	chr2R	—	6	7357590	7357714	7360081	7360205	0.611

(*Table continues*.)

Table 6. Continued

Genotype comparison	Gene	chr	Strand	MXE exon position	1st exon start	1st exon end	2nd exon start	2nd exon end	δ PSI
APPvsWT	Dscam1	chr2R	—	6	7358806	7358930	7359441	7359565	−0.619
APPTip60vsAPP	Dscam1	chr2R	—	6	7358806	7358930	7359441	7359565	0.417
APPvsWT	Dscam1	chr2R	—	6	7359441	7359565	7360290	7360414	0.813
APPTip60vsAPP	Dscam1	chr2R	—	6	7359441	7359565	7360290	7360414	−0.458

Differential splicing isoforms were quantified as percent spliced in (PSI) using rMATS. Difference in MXE isoform abundance between genotypes APP versus wild type and APP;Tip60 versus APP is reported as δ PSI.

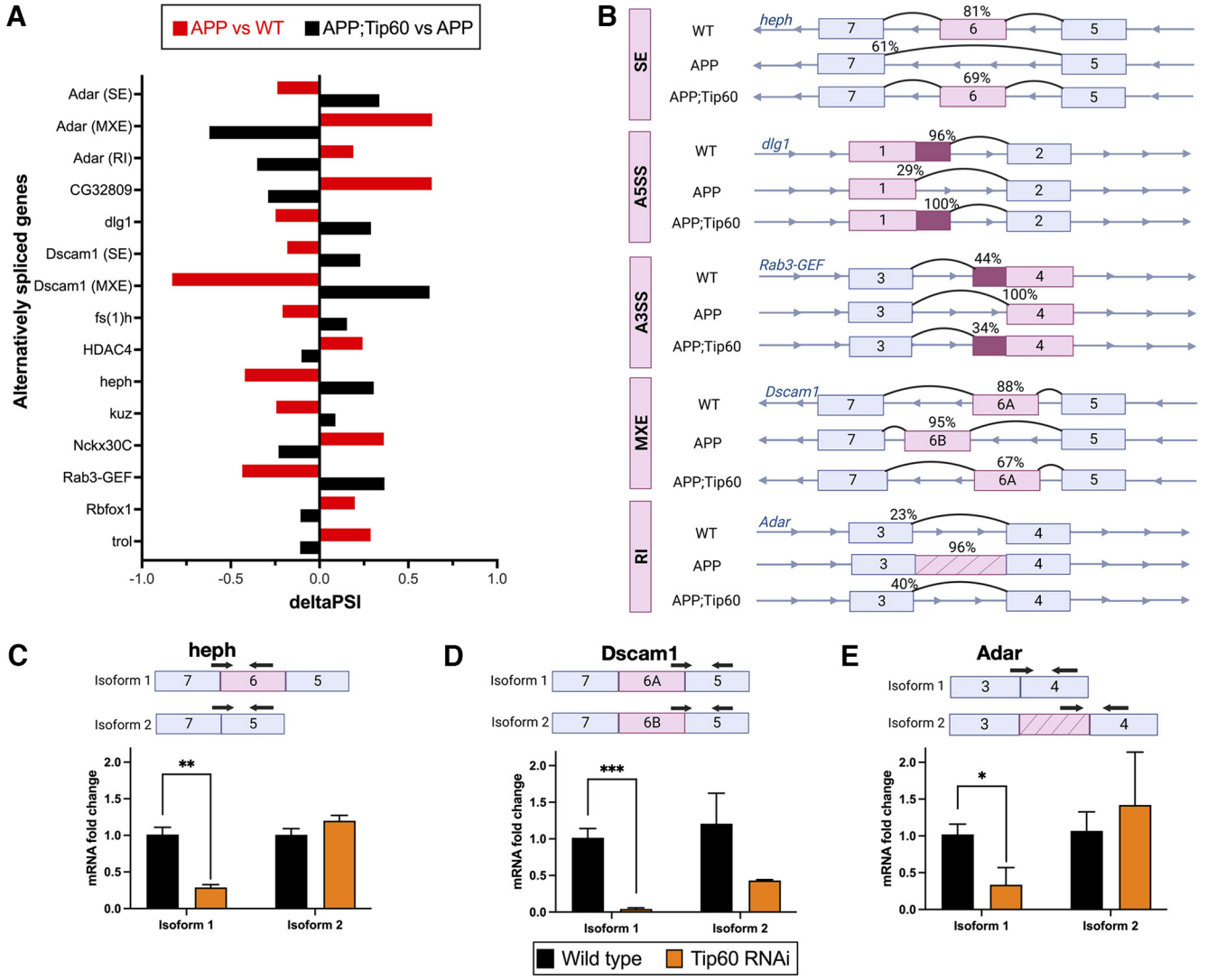

Figure 12. Tip60 modulates alternative splicing decisions of Alzheimer's disease (AD)-associated genes. ***A***, The 15 triaged Tip60-rescued splicing defects in AD-associated genes. *x*-axis represents differences in relative isoform abundance (ΔPSI, where PSI = percent spliced in) between APP versus wild type (red) and APP;Tip60 versus APP (black). ***B***, Schematic representation of Tip60-rescued splicing events from every type of alternative splicing. Percentage represents the relative isoform abundance for the indicated genotype obtained via rMATS analysis. ***C–E***, Splice-specific RT-qPCR on *Drosophila* larval brains from wild-type and Tip60 RNAi-mediated knock-down ($n = 3$) to detect alternatively spliced isoforms in heph, Dscam1, and Adar genes. Histogram represents relative fold change in mRNA expression calculated using ddCT method using Rpl32 as the housekeeping gene. Statistical significance was calculated using unpaired Student's *t* test. $^{*}p < 0.05$, $^{**}p < 0.01$, $^{***}p < 0.001$. Error bars indicate SEM.

is altered in AD hippocampus, we propose that Tip60-mediated AS modulation is a conserved critical posttranscriptional step that is disrupted early in AD etiology. In particular, we find Tip60-RNA binding of ADAM10, a constitutive α-secretase, is significantly lost under AD pathology. Interestingly, reduced ADAM10 activity in the postmortem human AD brain has been linked to AS induced isoform change without a change in the overall gene expression (Marques-Coelho et al., 2021), suggesting Tip60 modulated ADAM10 splicing could be central to AD pathogenesis. Thus, we are the first to uncover distinct histone and RNA binding capabilities for Tip60 that mediate its function in neural gene control and RNA splicing, respectively, and may underly the chromatin packaging and splicing defects that are now characterized as hallmarks of AD.

One target, two functions: Tip60 HAT as a novel therapeutic target for Alzheimer's disease

Pharmacological treatments aiming to restore histone acetylation via HDAC inhibition are currently a research hotspot for developing AD cognition enhancing drugs (Gräff and Tsai, 2013;

A

	Drosophila			Human ortholog		
No.	Gene	Splicing event	Splice site	Gene	Biological function	Splicing defects in AD brain
1.	Adar	SE MXE RI	Exon 3 Exon at 2 Between 3 & 4	ADARB1	Adenosine to inosine RNA editing and alternative splicing	Yes^{+}
2.	CG32809	A5SS or A3SS	Exon 1 or 3	KIAA1217	Skeletal system development	--
3.	dlg1	A5SS	Exon 1	DLG1	Synaptic scaffolding; APP metabolism	Yes$^{+*\wedge"}$
4.	Dscam1	SE MXE	Exon 9 Exon at 6	DSCAML1	Neuron cell adhesion and axon guidance	--
5.	fs(1)h	A5SS	Exon 1	BRD2	Chromatin remodeling and regulation of transcription	Yes^{+*}
6.	HDAC4	A3SS or MXE	Exon 3 or 5	HDAC4	Histone deacetylation mediated gene repression	--
7.	heph	SE	Exon 6	PTBP1	RNA alternative splicing and mRNA processing	Yes$^{+*\wedge"}$
8.	kuz	SE	Exon 3 or 12	ADAM10	α-secretase; Non-amyloidogenic APP cleavage	Yes^{+}
9.	Nckx30C	A3SS	Exon 1 or 2	SLC24A2	Calcium signaling for learning and memory	--
10.	Rab3-GEF	A3SS	Exon 4	MADD	Rab3 GDP to GTP activation; Cell apoptosis	Yes$^{+*\wedge}$
11.	Rbfox1	MXE	Exon at 3 or 9	RBFOX1	RNA alternative splicing and mRNA processing	--
12.	trol	SE	Exon 20	HSPG2	Cell-surface receptor signaling; amyloid-beta binding	Yes^{+}

B

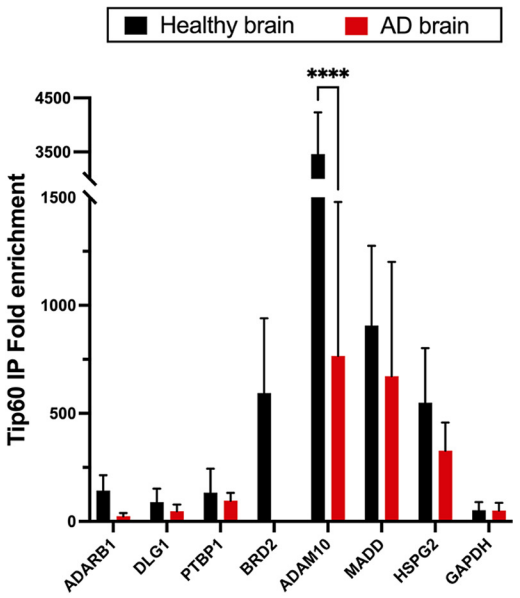

Figure 13. Tip60-RNA targeting is conserved in human hippocampus and impaired in Alzheimer's disease (AD) patient hippocampus. ***A***, Conserved human orthologs for the 12 triaged AD-associated Tip60-rescued genes were predicted using DIOPT. Previously reported splicing defects in postmortem human AD brain tissues were identified in the literature: $^{+}$Marques-Coelho et al. (2021), *Adusumalli et al. (2019), ^Tollervey et al. (2011), "Raj et al. (2018). ***B***, Tip60-bound RNA immunoprecipitation and RT-qPCR (RIP-qPCR) was performed on hippocampus obtained from healthy controls or AD patients ($n = 3$ brains). Histogram represents Tip60 IP fold enrichment for each gene relative to Rabbit IgG (negative control). Statistical significance was calculated using two-way ANOVA with Sidak's multiple comparison test. ****$p < 0.001$. Error bars indicate SEM.

Simões-Pires et al., 2013; Mielcarek et al., 2015). Although promising in reinstating cognition, HDAC inhibitors are known to exhibit side effects because of nonspecific global hyperacetylation (Didonna and Opal, 2015; Yang et al., 2017). Alternatively, enhancing activity of specific HATs in promoting cognition associated histone acetylation serves as an exciting new therapeutic strategy that remains to be fully explored (Caccamo et al., 2010; Selvi et al., 2010; Valor et al., 2013). In support of this concept, here we identify a novel splicing modulation function for Tip60 that likely complements its histone function for neuroprotection, therefore highlighting Tip60 as unique dual-functioning therapeutic target for ameliorating both, histone and splicing aberrations in AD. Strikingly, mutations only in RNA-binding and not histone-binding residues in the Esa1 HAT chromodomain are lethal (Shimojo et al., 2008), strongly supporting that the RNA function of HATs are nonredundant and critical for viability. Although precise mechanisms underlying Tip60-mediated AS regulation remain to be elucidated, we propose three probable mechanisms. First, similar to RNA-binding proteins (Herzel et al., 2017; Rachez et al., 2021), Tip60 could be binding at a splice site or an accessory site influencing transient RNA folding, and therefore, may modulate the timing of splice site exposure to the splicing machinery. Second, since Tip60 typically interacts with additional proteins in a complex for gene regulation (Ikura et al., 2000; Frank et al., 2003), Tip60-RNA binding could trigger assembly of a secondary complex that ultimately modulates AS decisions. Third, since histone acetylation modifications have been implicated in AS regulation

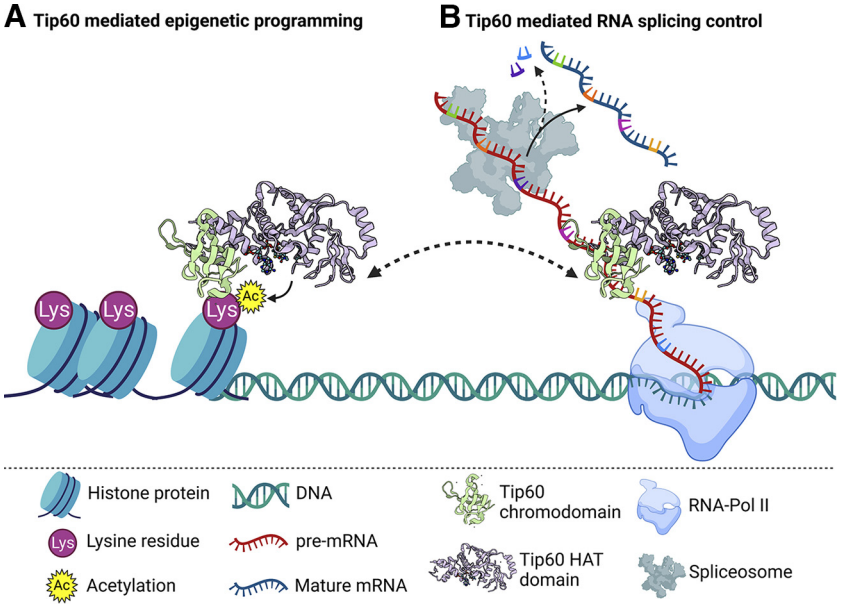

Figure 14. Model for Tip60's novel bi-level gene regulation at the chromatin and RNA level. Our results support a model by which Tip60 regulates both, the expression and splicing of a similar set of neural targets via its functions at the chromatin and the RNA, respectively. ***A***, Tip60 promotes neural gene expression via histone acetylation at the chromatin that increases chromatin accessibility for the transcriptional machinery. ***B***, Tip60 targets the newly transcribed pre-mRNA to modulate its alternative splicing decision by either altering splice site accessibility, assembling a complex that affects splicing, or tethering it to the chromatin for splicing regulation via histone acetylation. The model figure was created using BioRender.

(Hnilicová et al., 2011; Rahhal and Seto, 2019), Tip60's HAT function might modulate AS decisions while it tethers the target pre-mRNA to the chromatin. Further, we observed Tip60-rescued AS events in two major splicing regulators, RBFOX1 and PTBP1 that could in turn impact splicing of other neural genes. Nevertheless, we do not rule out potential additional mechanisms. Our findings strongly underscore supplementing current histone acetylation targeted therapeutics with splice-switching strategies, such as the use of antisense oligonucleotides (AO) that for desired pre-mRNA processing (Quemener et al., 2020; D. Li et al., 2021). Currently, six splice-switching AO have been approved by the US FDA for mRNA manipulation in rare diseases (D. Li et al., 2021; Raguraman et al., 2021). Although successful in reducing Aβ production and ameliorating cognition in AD pre-clinical models (Huynh et al., 2017; Chang et al., 2018), further studies are needed to corroborate the effectiveness and safety of splice-switching AO in AD. Dissecting apart Tip60's histone versus RNA function and further elucidation of mechanisms underlying Tip60-mediated AS modulation should provide earlier, safer, and more selective ways for AD therapeutics in the clinical setting.

References

Adusumalli S, Ngian ZK, Lin WQ, Benoukraf T, Ong CT (2019) Increased intron retention is a post-transcriptional signature associated with progressive aging and Alzheimer's disease. Aging cell 18:e12928.

Agirre E, Oldfield AJ, Bellora N, Segelle A, Luco RF (2021) Splicing-associated chromatin signatures: a combinatorial and position-dependent role for histone marks in splicing definition. Nat Commun 12:682.

Akhtar A, Zink D, Becker PB (2000) Chromodomains are protein–RNA interaction modules. Nature 407:405–409.

Akoury E, Ma G, Demolin S, Brönner C, Zocco M, Cirilo A, Ivic N, Halic M (2019) Disordered region of H3K9 methyltransferase Clr4 binds the nucleosome and contributes to its activity. Nucleic Acids Res 47:6726–6736.

Alam S, Suzuki H, Tsukahara T (2014) Alternative splicing regulation of APP exon 7 by RBFox proteins. Neurochem Int 78:7–17.

Annese A, Manzari C, Lionetti C, Picardi E, Horner DS, Chiara M, Caratozzolo MF, Tullo A, Fosso B, Pesole G, D'erchia AM (2018) Whole transcriptome profiling of late-onset Alzheimer's disease patients provides insights into the molecular changes involved in the disease. Sci Rep 8:4282.

Beaver M, Bhatnagar A, Panikker P, Zhang H, Snook R, Parmar V, Vijayakumar G, Betini N, Akhter S, Elefant F (2020) Disruption of Tip60 HAT mediated neural histone acetylation homeostasis is an early common event in neurodegenerative diseases. Sci Rep 10:18265.

Beaver M, Karisetty BC, Zhang H, Bhatnagar A, Armour E, Parmar V, Brown R, Xiang M, Elefant F (2021) Chromatin and transcriptomic profiling uncover dysregulation of the Tip60 HAT/HDAC2 epigenomic landscape in the neurodegenerative brain. Epigenetics 17:786–807.

Belyaev ND, Kellett KA, Beckett C, Makova NZ, Revett TJ, Nalivaeva NN, Hooper NM, Turner AJ (2010) The transcriptionally active amyloid precursor protein (APP) intracellular domain is preferentially produced from the 695 isoform of APP in a β-secretase-dependent pathway. J Biol Chem 285:41443–41454.

Bernstein E, Allis CD (2005) RNA meets chromatin. Genes Dev 19:1635–1655.

Bernstein E, Duncan EM, Masui O, Gil J, Heard E, Allis CD (2006) Mouse polycomb proteins bind differentially to methylated histone H3 and RNA and are enriched in facultative heterochromatin. Mol Cell Biol 26:2560–2569.

Bhatia SS, Koeffler HP, Jha S (2020) Abstract 4670: TIP60 regulates alternative splicing of Integrin subunit alpha 6. Cancer Res 80:4670–4670.

Bhatnagar A, Karnay AM, Elefant F (2023) *Drosophila* epigenetics. In: Handbook of epigenetics, pp 215–247. Amsterdam: Elsevier.

Caccamo A, Maldonado MA, Bokov AF, Majumder S, Oddo S (2010) CBP gene transfer increases BDNF levels and ameliorates learning and memory deficits in a mouse model of Alzheimer's disease. Proc Natl Acad Sci U S A 107:22687–22692.

Chang JL, Hinrich AJ, Roman B, Norrbom M, Rigo F, Marr RA, Norstrom EM, Hastings ML (2018) Targeting amyloid-β precursor protein, APP, splicing with antisense oligonucleotides reduces toxic amyloid-β production. Mol Ther 26:1539–1551.

Chen EY, Tan CM, Kou Y, Duan Q, Wang Z, Meirelles GV, Clark NR, Ma'ayan A (2013) Enrichr: interactive and collaborative HTML5 gene list enrichment analysis tool. BMC Bioinformatics 14:128.

Chen Y, Varani G (2005) Protein families and RNA recognition. FEBS J 272:2088–2097.

Chen Y, Chen Y, Shi C, Huang Z, Zhang Y, Li S, Li Y, Ye J, Yu C, Li Z, Zhang X, Wang J, Yang H, Fang L, Chen Q (2018) SOAPnuke: a MapReduce acceleration-supported software for integrated quality control and preprocessing of high-throughput sequencing data. Gigascience 7:1–6.

Corley M, Burns MC, Yeo GW (2020) How RNA-binding proteins interact with RNA: molecules and mechanisms. Mol Cell 78:9–29.

Delano WL (2002) Pymol: an open-source molecular graphics tool. CCP4 Newsl. Protein Crystallogr 40:82–92.

Del Villar K, Miller CA (2004) Down-regulation of DENN/MADD, a TNF receptor binding protein, correlates with neuronal cell death in Alzheimer's disease brain and hippocampal neurons. Proc Natl Acad Sci U S A 101:4210–4215.

Deture MA, Dickson DW (2019) The neuropathological diagnosis of Alzheimer's disease. Mol Neurodegener 14:32.

Didonna A, Opal P (2015) The promise and perils of HDAC inhibitors in neurodegeneration. Ann Clin Transl Neurol 2:79–101.

Dobin A, Davis CA, Schlesinger F, Drenkow J, Zaleski C, Jha S, Batut P, Chaisson M, Gingeras TR (2013) STAR: ultrafast universal RNA-seq aligner. Bioinformatics 29:15–21.

Ewels P, Magnusson M, Lundin S, Käller M (2016) MultiQC: summarize analysis results for multiple tools and samples in a single report. Bioinformatics 32:3047–3048.

Francis YI, Fà M, Ashraf H, Zhang H, Staniszewski A, Latchman DS, Arancio O (2009) Dysregulation of histone acetylation in the APP/PS1 mouse model of Alzheimer's disease. J Alzheimers Dis 18:131–139.

Frank SR, Parisi T, Taubert S, Fernandez P, Fuchs M, Chan HM, Livingston DM, Amati B (2003) MYC recruits the TIP60 histone acetyltransferase complex to chromatin. EMBO Rep 4:575–580.

Gräff J, Tsai LH (2013) The potential of HDAC inhibitors as cognitive enhancers. Annu Rev Pharmacol Toxicol 53:311–330.

Gräff J, Rei D, Guan JS, Wang WY, Seo J, Hennig KM, Nieland TJ, Fass DM, Kao PF, Kahn M, Su SC, Samiei A, Joseph N, Haggarty SJ, Delalle I, Tsai LH (2012) An epigenetic blockade of cognitive functions in the neurodegenerating brain. Nature 483:222–226.

Graveley BR (2005) Mutually exclusive splicing of the insect Dscam pre-mRNA directed by competing intronic RNA secondary structures. Cell 123:65–73.

Hassan M, Zahid S, Alashwal H, Kloczkowski A, Moustafa AA (2021) Mechanistic insights into TNFR1/MADD death domains in Alzheimer's disease through conformational molecular dynamic analysis. Scientific Reports 11:12256.

Herzel L, Ottoz DSM, Alpert T, Neugebauer KM (2017) Splicing and transcription touch base: co-transcriptional spliceosome assembly and function. Nat Rev Mol Cell Biol 18:637–650.

Hnilicová J, Hozeifi S, Dušková E, Icha J, Tománková T, Staněk D (2011) Histone deacetylase activity modulates alternative splicing. PLoS One 6:e16727.

Hu Y, Flockhart I, Vinayagam A, Bergwitz C, Berger B, Perrimon N, Mohr SE (2011) An integrative approach to ortholog prediction for disease-focused and other functional studies. BMC Bioinformatics 12:1–16.

Huynh TV, Liao F, Francis CM, Robinson GO, Serrano JR, Jiang H, Roh J, Finn MB, Sullivan PM, Esparza TJ, Stewart FR, Mahan TE, Ulrich JD, Cole T, Holtzman DM (2017) Age-dependent effects of apoE reduction using antisense oligonucleotides in a model of β-amyloidosis. Neuron 96:1013–1023.e1014.

Ikura T, Ogryzko VV, Grigoriev M, Groisman R, Wang J, Horikoshi M, Scully R, Qin J, Nakatani Y (2000) Involvement of the TIP60 histone acetylase complex in DNA repair and apoptosis. Cell 102:463–473.

Ishida M, Shimojo H, Hayashi A, Kawaguchi R, Ohtani Y, Uegaki K, Nishimura Y, Nakayama J-I (2012) Intrinsic nucleic acid-binding activity

of Chp1 chromodomain is required for heterochromatic gene silencing. Mol Cell 47:228–241.
Jakubauskienė E, Kanopka A (2021) Alternative splicing and hypoxia puzzle in Alzheimer's and Parkinson's diseases. Genes 12:1272.
Johansen KM, Cai W, Deng H, Bao X, Zhang W, Girton J, Johansen J (2009) Polytene chromosome squash methods for studying transcription and epigenetic chromatin modification in *Drosophila* using antibodies. Methods 48:387–397.
Johnson AA, Sarthi J, Pirooznia SK, Reube W, Elefant F (2013) Increasing Tip60 HAT levels rescues axonal transport defects and associated behavioral phenotypes in a *Drosophila* Alzheimer's disease model. J Neurosci 33:7535–7547.
Karnay A, Karisetty BC, Beaver M, Elefant F (2019) Hippocampal stimulation promotes intracellular Tip60 dynamics with concomitant genome reorganization and synaptic gene activation. Mol Cell Neurosci 101:103412.
Keller C, Adaixo R, Stunnenberg R, Woolcock KJ, Hiller S, Bühler M (2012) HP1(Swi6) mediates the recognition and destruction of heterochromatic RNA transcripts. Mol Cell 47:215–227.
Khermesh K, D'erchia AM, Barak M, Annese A, Wachtel C, Levanon EY, Picardi E, Eisenberg E (2016) Reduced levels of protein recoding by A-to-I RNA editing in Alzheimer's disease. RNA 22:290–302.
Killin LO, Starr JM, Shiue IJ, Russ TC (2016) Environmental risk factors for dementia: a systematic review. BMC Geriatr 16:175.
Kim CH, Kim JW, Jang SM, An JH, Seo SB, Choi KH (2015) The chromodomain-containing histone acetyltransferase TIP60 acts as a code reader, recognizing the epigenetic codes for initiating transcription. Biosci Biotechnol Biochem 79:532–538.
Kim D, Paggi JM, Park C, Bennett C, Salzberg SL (2019) Graph-based genome alignment and genotyping with HISAT2 and HISAT-genotype. Nat Biotechnol 37:907–915.
Knopman DS, Amieva H, Petersen RC, Chételat G, Holtzman DM, Hyman BT, Nixon RA, Jones DT (2021) Alzheimer disease. Nat Rev Dis Primers 7:33.
Krieger E, Joo K, Lee J, Lee J, Raman S, Thompson J, Tyka M, Baker D, Karplus K (2009) Improving physical realism, stereochemistry, and side-chain accuracy in homology modeling: four approaches that performed well in CASP8. Proteins 77 [Suppl 9]:114–122.
Langmead B, Salzberg SL (2012) Fast gapped-read alignment with Bowtie 2. Nat Methods 9:357–359.
Laskowski RA, Macarthur MW, Moss DS, Thornton JM (1993) PROCHECK: a program to check the stereochemical quality of protein structures. J Appl Crystallogr 26:283–291.
Letunic I, Bork P (2018) 20 years of the SMART protein domain annotation resource. Nucleic Acids Res 46:D493–D496.
Li B, Dewey CN (2011) RSEM: accurate transcript quantification from RNA-Seq data with or without a reference genome. BMC Bioinformatics 12:323.
Li D, Mcintosh CS, Mastaglia FL, Wilton SD, Aung-Htut MT (2021) Neurodegenerative diseases: a hotbed for splicing defects and the potential therapies. Transl Neurodegener 10:16.
Li Q, Lee JA, Black DL (2007) Neuronal regulation of alternative pre-mRNA splicing. Nat Rev Neurosci 8:819–831.
Liu CC, Zhao N, Yamaguchi Y, Cirrito JR, Kanekiyo T, Holtzman DM, Bu G (2016) Neuronal heparan sulfates promote amyloid pathology by modulating brain amyloid-β clearance and aggregation in Alzheimer's disease. Sci Transl Med 8:332ra344.
Liu X, Jiao B, Shen L (2018) The epigenetics of Alzheimer's disease: factors and therapeutic implications. Front Genet 9:579–579.
Love JE, Hayden EJ, Rohn TT (2015) Alternative splicing in Alzheimer's disease. J Parkinsons Dis Alzheimers Dis 2:6.
Lu X, Deng Y, Yu D, Cao H, Wang L, Liu L, Yu C, Zhang Y, Guo X, Yu G (2014) Histone acetyltransferase p300 mediates histone acetylation of PS1 and BACE1 in a cellular model of Alzheimer's disease. PLoS One 9: e103067.
Luco RF, Allo M, Schor IE, Kornblihtt AR, Misteli T (2011) Epigenetics in alternative pre-mRNA splicing. Cell 144:16–26.
Manzine PR, Ettcheto M, Cano A, Busquets O, Marcello E, Pelucchi S, Di Luca M, Endres K, Olloquequi J, Camins A, Cominetti MR (2019) ADAM10 in Alzheimer's disease: pharmacological modulation by natural compounds and its role as a peripheral marker. Biomed Pharmacother 113:108661.
Marcello E, Saraceno C, Musardo S, Vara H, De La Fuente AG, Pelucchi S, Di Marino D, Borroni B, Tramontano A, Pérez-Otaño I, Padovani A, Giustetto M, Gardoni F, Di Luca M (2013) Endocytosis of synaptic ADAM10 in neuronal plasticity and Alzheimer's disease. J Clin Invest 123:2523–2538.
Marques-Coelho D, Iohan LDCC, Melo De Farias AR, Flaig A; Brainbank Neuro–CEB Neuropathology Network; Lambert JC, Costa MR (2021) Differential transcript usage unravels gene expression alterations in Alzheimer's disease human brains. NPJ Aging Mech Dis 7:2.
Mielcarek M, Zielonka D, Carnemolla A, Marcinkowski JT, Guidez F (2015) HDAC4 as a potential therapeutic target in neurodegenerative diseases: a summary of recent achievements. Front Cell Neurosci 9:42.
Morales V, Regnard C, Izzo A, Vetter I, Becker PB (2005) The MRG domain mediates the functional integration of MSL3 into the dosage compensation complex. Mol Cell Biol 25:5947–5954.
Muppirala UK, Honavar VG, Dobbs D (2011) Predicting RNA-protein interactions using only sequence information. BMC Bioinformatics 12:489.
Nativio R, Donahue G, Berson A, Lan Y, Amlie-Wolf A, Tuzer F, Toledo JB, Gosai SJ, Gregory BD, Torres C, Trojanowski JQ, Wang L-S, Johnson FB, Bonini NM, Berger SL (2018) Dysregulation of the epigenetic landscape of normal aging in Alzheimer's disease. Nat Neurosci 21:497–505.
Niemitz E (2013) ADAM10 and Alzheimer's disease. Nat Genet 45:1273–1273.
O'Leary NA, et al. (2016) Reference sequence (RefSeq) database at NCBI: current status, taxonomic expansion, and functional annotation. Nucleic Acids Res 44:D733–D745.
Panikker P, Xu SJ, Zhang H, Sarthi J, Beaver M, Sheth A, Akhter S, Elefant F (2018) Restoring Tip60 HAT/HDAC2 balance in the neurodegenerative brain relieves epigenetic transcriptional repression and reinstates cognition. J Neurosci 38:4569–4583.
Peixoto L, Abel T (2013) The role of histone acetylation in memory formation and cognitive impairments. Neuropsychopharmacology 38:62–76.
Piñero J, Bravo À, Queralt-Rosinach N, Gutiérrez-Sacristán A, Deu-Pons J, Centeno E, García-García J, Sanz F, Furlong LI (2016) DisGeNET: a comprehensive platform integrating information on human disease-associated genes and variants. Nucleic Acids Res 45:D833–D839.
Pirooznia SK, Elefant F (2013) Targeting specific HATs for neurodegenerative disease treatment: translating basic biology to therapeutic possibilities. Front Cell Neurosci 7:30.
Pirooznia SK, Sarthi J, Johnson AA, Toth MS, Chiu K, Koduri S, Elefant F (2012) Tip60 HAT activity mediates APP induced lethality and apoptotic cell death in the CNS of a *Drosophila* Alzheimer's disease model. PLoS One 7:e41776.
Quemener AM, Bachelot L, Forestier A, Donnou-Fournet E, Gilot D, Galibert MD (2020) The powerful world of antisense oligonucleotides: from bench to bedside. Wiley Interdiscip Rev RNA 11:e1594.
Rachez C, Legendre R, Costallat M, Varet H, Yi J, Kornobis E, Muchardt C (2021) HP1γ binding pre-mRNA intronic repeats modulates RNA splicing decisions. EMBO Rep 22:e52320.
Raguraman P, Balachandran AA, Chen S, Diermeier SD, Veedu RN (2021) Antisense oligonucleotide-mediated splice switching: potential therapeutic approach for cancer mitigation. Cancers (Basel) 13:5555.
Rahhal R, Seto E (2019) Emerging roles of histone modifications and HDACs in RNA splicing. Nucleic Acids Res 47:4911–4926.
Raj T, Li YI, Wong G, Humphrey J, Wang M, Ramdhani S, Wang YC, Ng B, Gupta I, Haroutunian V, Schadt EE, Young-Pearse T, Mostafavi S, Zhang B, Sklar P, Bennett DA, De Jager PL (2018) Integrative transcriptome analyses of the aging brain implicate altered splicing in Alzheimer's disease susceptibility. Nat Genet 50:1584–1592.
Robert X, Gouet P (2014) Deciphering key features in protein structures with the new ENDscript server. Nucleic Acids Res 42:W320–W324.
Sanchez-Mut JV, Gräff J (2015) Epigenetic alterations in Alzheimer's disease. Front Behav Neurosci 9:347.
Sarthi J, Elefant F (2011) dTip60 HAT activity controls synaptic bouton expansion at the *Drosophila* neuromuscular junction. PLoS One 6: e26202.
Schirling C, Heseding C, Heise F, Kesper D, Klebes A, Klein-Hitpass L, Vortkamp A, Hoffmann D, Saumweber H, Ehrenhofer-Murray AE (2010) Widespread regulation of gene expression in the *Drosophila* genome by the histone acetyltransferase dTip60. Chromosoma 119:99–113.

Selvi BR, Cassel JC, Kundu TK, Boutillier AL (2010) Tuning acetylation levels with HAT activators: therapeutic strategy in neurodegenerative diseases. Biochim Biophys Acta 1799:840–853.

Shen S, Park JW, Lu Z-X, Lin L, Henry MD, Wu YN, Zhou Q, Xing Y (2014) rMATS: robust and flexible detection of differential alternative splicing from replicate RNA-Seq data. Proc Natl Acad Sci U S A 111:E5593–E5601.

Shen X, Chen J, Li J, Kofler J, Herrup K (2016) Neurons in vulnerable regions of the Alzheimer's disease brain display reduced ATM signaling. eNeuro 3:ENEURO.0124-15.2016.

Shimojo H, Sano N, Moriwaki Y, Okuda M, Horikoshi M, Nishimura Y (2008) Novel structural and functional mode of a knot essential for RNA binding activity of the Esa1 presumed chromodomain. J Mol Biol 378:987–1001.

Sievers F, Wilm A, Dineen D, Gibson TJ, Karplus K, Li W, Lopez R, McWilliam H, Remmert M, Söding J, Thompson JD, Higgins DG (2011) Fast, scalable generation of high-quality protein multiple sequence alignments using clustal omega. Mol Syst Biol 7:539.

Silva B, Niehage C, Maglione M, Hoflack B, Sigrist SJ, Wassmer T, Pavlowsky A, Preat T (2020) Interactions between amyloid precursor protein-like (APPL) and MAGUK scaffolding proteins contribute to appetitive long-term memory in *Drosophila melanogaster*. J Neurogenet 34:92–105.

Simões-Pires C, Zwick V, Nurisso A, Schenker E, Carrupt P-A, Cuendet M (2013) HDAC6 as a target for neurodegenerative diseases: what makes it different from the other HDACs? Mol Neurodegener 8:7.

Smith P, Al Hashimi A, Girard J, Delay C, Hébert SS (2011) In vivo regulation of amyloid precursor protein neuronal splicing by microRNAs. J Neurochem 116:240–247.

Solomon O, Oren S, Safran M, Deshet-Unger N, Akiva P, Jacob-Hirsch J, Cesarkas K, Kabesa R, Amariglio N, Unger R, Rechavi G, Eyal E (2013) Global regulation of alternative splicing by adenosine deaminase acting on RNA (ADAR). RNA 19:591–604.

Su CH, Dhananjaya D, Tarn WY (2018) Alternative splicing in neurogenesis and brain development. Front Mol Biosci 5:12.

Sun Y, Jiang X, Xu Y, Ayrapetov MK, Moreau LA, Whetstine JR, Price BD (2009) Histone H3 methylation links DNA damage detection to activation of the tumour suppressor Tip60. Nat Cell Biol 11:1376.

Teplova M, Malinina L, Darnell JC, Song J, Lu M, Abagyan R, Musunuru K, Teplov A, Burley SK, Darnell RB, Patel DJ (2011) Protein-RNA and protein-protein recognition by dual KH1/2 domains of the neuronal splicing factor Nova-1. Structure 19:930–944.

Tollervey JR, Wang Z, Hortobágyi T, Witten JT, Zarnack K, Kayikci M, Clark TA, Schweitzer AC, Rot G, Curk T, Zupan B, Rogelj B, Shaw CE, Ule J (2011) Analysis of alternative splicing associated with aging and neurodegeneration in the human brain. Genome Res 21:1572–1582.

UniProt Consortium (2020) UniProt: the universal protein knowledgebase in 2021. Nucleic Acids Res 49:D480–D489.

Valor LM, Viosca J, Lopez-Atalaya JP, Barco A (2013) Lysine acetyltransferases CBP and p300 as therapeutic targets in cognitive and neurodegenerative disorders. Curr Pharm Des 19:5051–5064.

Van Gool D, David G, Lammens M, Baro F, Dom R (1993) Heparan sulfate expression patterns in the amyloid deposits of patients with Alzheimer's and Lewy body type dementia. Dementia 4:308–314.

Vatolina TY, Boldyreva LV, Demakova OV, Demakov SA, Kokoza EB, Semeshin VF, Babenko VN, Goncharov FP, Belyaeva ES, Zhimulev IF (2011) Identical functional organization of nonpolytene and polytene chromosomes in *Drosophila melanogaster*. PLoS One 6:e25960.

Wang L, Wang S, Li W (2012) RSeQC: quality control of RNA-seq experiments. Bioinformatics 28:2184–2185.

Waterhouse AM, Procter JB, Martin DMA, Clamp M, Barton GJ (2009) Jalview version 2—a multiple sequence alignment editor and analysis workbench. Bioinformatics 25:1189–1191.

Waterhouse A, Bertoni M, Bienert S, Studer G, Tauriello G, Gumienny R, Heer FT, de Beer TAP, Rempfer C, Bordoli L, Lepore R, Schwede T (2018) SWISS-MODEL: homology modelling of protein structures and complexes. Nucleic Acids Res 46:W296–W303.

Xu S, Wilf R, Menon T, Panikker P, Sarthi J, Elefant F (2014) Epigenetic control of learning and memory in *Drosophila* by Tip60 HAT action. Genetics 198:1571–1586.

Xu S, Panikker P, Iqbal S, Elefant F (2016) Tip60 HAT action mediates environmental enrichment induced cognitive restoration. PLoS One 11: e0159623.

Xu SJ, Lombroso SI, Fischer DK, Carpenter MD, Marchione DM, Hamilton PJ, Lim CJ, Neve RL, Garcia BA, Wimmer ME, Pierce RC, Heller EA (2021) Chromatin-mediated alternative splicing regulates cocaine-reward behavior. Neuron 109:2943–2966.e8.

Yang SS, Zhang R, Wang G, Zhang YF (2017) The development prospection of HDAC inhibitors as a potential therapeutic direction in Alzheimer's disease. Transl Neurodegener 6:19.

Yuan XZ, Sun S, Tan CC, Yu JT, Tan L (2017) The role of ADAM10 in Alzheimer's disease. J Alzheimers Dis 58:303–322.

Zhang GL, Zhang X, Wang XM, Li JP (2014) Towards understanding the roles of heparan sulfate proteoglycans in Alzheimer's disease. Biomed Res Int 2014:516028.

Zhang H, Karisetty BC, Bhatnagar A, Armour EM, Beaver M, Roach TV, Mortazavi S, Mandloi S, Elefant F (2020) Tip60 protects against amyloid-β-induced transcriptomic alterations via different modes of action in early versus late stages of neurodegeneration. Mol Cell Neurosci 109:103570.

Zhang Y, Lei M, Yang X, Feng Y, Yang Y, Loppnau P, Li Y, Yang Y, Min J, Liu Y (2018) Structural and histone binding studies of the chromo barrel domain of TIP 60. FEBS Lett 592:1221–1232.

Zhu X, Singh N, Donnelly C, Boimel P, Elefant F (2007) The cloning and characterization of the histone acetyltransferase human homolog Dmel\TIP60 in *Drosophila melanogaster*: dmel\TIP60 is essential for multicellular development. Genetics 175:1229–1240.